DESY 94-032

Measurement of Total and Partial Photon Proton Cross Sections at 180 GeV Center of Mass Energy

ZEUS Collaboration

Abstract

Photon proton cross sections for elastic light vector meson production, $\sigma_{el}^{\gamma p}$, inelastic diffractive production, $\sigma_{d}^{\gamma p}$, non-diffractive production, $\sigma_{nd}^{\gamma p}$, as well as the total cross section, $\sigma_{tot}^{\gamma p}$, have been measured at an average γp center of mass energy of 180 GeV with the ZEUS detector at HERA. The resulting values are $\sigma_{el}^{\gamma p} = 18 \pm 7$ μb, $\sigma_{d}^{\gamma p} = 33 \pm 8$ μb, $\sigma_{nd}^{\gamma p} = 91 \pm 11$ μb, and $\sigma_{tot}^{\gamma p} = 143 \pm 17$ μb, where the errors include statistical and systematic errors added in quadrature.

The ZEUS Collaboration

M. Derrick, D. Krakauer, S. Magill, B. Musgrave, J. Repond, J. Schlereth, R. Stanek, R.L. Talaga, J. Thron
Argonne National Laboratory, Argonne, IL, USA [p]

F. Arzarello, R. Ayad[1], G. Bari, M. Basile, L. Bellagamba, D. Boscherini, A. Bruni, G. Bruni, P. Bruni, G. Cara Romeo, G. Castellini[2], M. Chiarini, L. Cifarelli[3], F. Cindolo, F. Ciralli, A. Contin, S. D'Auria, C. Del Papa, F. Frasconi, P. Giusti, G. Iacobucci, G. Laurenti, G. Levi, G. Maccarrone, A. Margotti, T. Massam, R. Nania, C. Nemoz, F. Palmonari, G. Sartorelli, R. Timellini, Y. Zamora Garcia[1], A. Zichichi
University and INFN Bologna, Bologna, Italy [f]

A. Bargende, J. Crittenden, K. Desch, B. Diekmann, T. Doeker, L. Feld, A. Frey, M. Geerts, G. Geitz, H. Hartmann, D. Haun, K. Heinloth, E. Hilger, H.-P. Jakob, U.F. Katz, S. Kramarczyk[4], A. Mass, S. Mengel, J. Mollen, E. Paul, Ch. Rembser, R. Schattevoy, J.-L. Schneider, D. Schramm, R. Wedemeyer
Physikalisches Institut der Universität Bonn, Bonn, Federal Republic of Germany [c]

A. Cassidy, D.G. Cussans[5], N. Dyce, B. Foster, S. George, R. Gilmore, G.P. Heath, H.F. Heath, M. Lancaster, T.J. Llewellyn, C.J.S. Morgado, J.A. O'Mara, R.J. Tapper, S.S. Wilson, R. Yoshida
H.H. Wills Physics Laboratory, University of Bristol, Bristol, U.K. [o]

R.R. Rau
Brookhaven National Laboratory, Upton, L.I., USA [p]

M. Arneodo, M. Schioppa, G. Susinno
Calabria University, Physics Dept.and INFN, Cosenza, Italy [f]

A. Bernstein, A. Caldwell, I. Gialas, J.A. Parsons, S. Ritz, F. Sciulli, P.B. Straub, L. Wai, S. Yang
Columbia University, Nevis Labs., Irvington on Hudson, N.Y., USA [q]

P. Borzemski, J. Chwastowski, A. Eskreys, K. Piotrzkowski, M. Zachara, L. Zawiejski
Inst. of Nuclear Physics, Cracow, Poland [j]

L. Adamczyk, B. Bednarek, K. Eskreys, K. Jeleń, D. Kisielewska, T. Kowalski, E. Rulikowska-Zarębska, L. Suszycki, J. Zając
Faculty of Physics and Nuclear Techniques, Academy of Mining and Metallurgy, Cracow, Poland [j]

T. Kędzierski, A. Kotański, M. Przybycień
Jagellonian Univ., Dept. of Physics, Cracow, Poland [k]

L.A.T. Bauerdick, U. Behrens, J.K. Bienlein, S. Böttcher, C. Coldewey, G. Drews, M. Flasiński[6], I. Fleck, D.J. Gilkinson, P. Göttlicher, B. Gutjahr, T. Haas, L. Hagge, W. Hain, D. Hasell, H. Heßling, H. Hultschig, P. Joos, M. Kasemann, R. Klanner, W. Koch, L. Köpke, U. Kötz, H. Kowalski, W. Kröger, J. Krüger[4], J. Labs, A. Ladage, B. Löhr, M. Löwe, D. Lüke, J. Mainusch, O. Mańczak, J.S.T. Ng, S. Nickel, D. Notz, K. Ohrenberg, M. Rohde, J. Roldán[7], U. Schneekloth, J. Schroeder, W. Schulz, F. Selonke, E. Stiliaris[7], T. Tsurugai, W. Vogel[8], D. Westphal, G. Wolf, C. Youngman
Deutsches Elektronen-Synchrotron DESY, Hamburg, Federal Republic of Germany

H.J. Grabosch, A. Leich, A. Meyer, C. Rethfeldt, S. Schlenstedt
DESY-Zeuthen, Inst. für Hochenergiephysik, Zeuthen, Federal Republic of Germany

G. Barbagli, M. Nuti, P. Pelfer
University and INFN, Florence, Italy [f]

G. Anzivino, S. De Pasquale, S. Qian, L. Votano
INFN, Laboratori Nazionali di Frascati, Frascati, Italy [f]

A. Bamberger, A. Freidhof, T. Poser[9], S. Söldner-Rembold, G. Theisen, T. Trefzger
Fakultät für Physik der Universität Freiburg i.Br., Freiburg i.Br., Federal Republic of Germany [c]

N.H. Brook, P.J. Bussey, A.T. Doyle, J.R. Forbes, V.A. Jamieson, C. Raine, D.H. Saxon,
M. Stavrianakou, A.S. Wilson
Dept. of Physics and Astronomy, University of Glasgow, Glasgow, U.K. [o]

A. Dannemann, U. Holm, D. Horstmann, H. Kammerlocher[9], B. Krebs[10], T. Neumann, R. Sinkus, K. Wick
Hamburg University, I. Institute of Exp. Physics, Hamburg, Federal Republic of Germany [c]

E. Badura, B.D. Burow, A. Fürtjes[11], E. Lohrmann, J. Milewski, M. Nakahata[12], N. Pavel, G. Poelz, W. Schott,
J. Terron[7], F. Zetsche
Hamburg University, II. Institute of Exp. Physics, Hamburg, Federal Republic of Germany [c]

T.C. Bacon, R. Beuselinck, I. Butterworth, E. Gallo, V.L. Harris, K.R. Long, D.B. Miller, A. Prinias,
J.K. Sedgbeer, A. Vorvolakos, A. Whitfield
Imperial College London, High Energy Nuclear Physics Group, London, U.K. [o]

T. Bienz[13], H. Kreutzmann[14], U. Mallik, E. McCliment, M. Roco, M.Z. Wang
University of Iowa, Physics and Astronomy Dept., Iowa City, USA [p]

P. Cloth, D. Filges
Forschungszentrum Jülich, Institut für Kernphysik, Jülich, Federal Republic of Germany

S.H. An, S.M. Hong, C.O. Kim, T.Y. Kim, S.W. Nam, S.K. Park, M.H. Suh, S.H. Yon
Korea University, Seoul, Korea [h]

R. Imlay, S. Kartik, H.-J. Kim, R.R. McNeil, W. Metcalf, V.K. Nadendla
Louisiana State University, Dept. of Physics and Astronomy, Baton Rouge, LA, USA [p]

F. Barreiro[15], G. Cases, R. Graciani, J.M. Hernández, L. Hervás[16], L. Labarga[16], J. del Peso, J. Puga,
J.F. de Trocóniz[17]
Univer. Autónoma Madrid, Depto de Física Teóríca, Madrid, Spain [n]

F. Ikraiam, J.K. Mayer, G.R. Smith
University of Manitoba, Dept. of Physics, Winnipeg, Manitoba, Canada [a]

F. Corriveau, D.S. Hanna, J. Hartmann, L.W. Hung, J.N. Lim, C.G. Matthews, J.W. Mitchell[18], P.M. Patel,
L.E. Sinclair, D.G. Stairs, M. St.Laurent, R. Ullmann
McGill University, Dept. of Physics, Montreal, Quebec, Canada [a, b]

V. Bashkirov, B.A. Dolgoshein, A. Stifutkin
Moscow Engineering Physics Institute, Mosocw, Russia [l]

G.L. Bashindzhagyan, P.F. Ermolov, L.K. Gladilin, Y.A. Golubkov, V.D. Kobrin, V.A. Kuzmin, E.N. Kuznetsov,
A.A. Savin, A.N. Solomin, A.G. Voronin, N.P. Zotov
Moscow State University, Institute of Nuclear Pysics, Moscow, Russia [m]

S. Bentvelsen, M. Botje, F. Chlebana, A. Dake, J. Engelen, P. de Jong[19], M. de Kamps, P. Kooijman, A. Kruse,
V. O'Dell[20], A. Tenner, H. Tiecke, W. Verkerke, M. Vreeswijk, L. Wiggers, E. de Wolf, R. van Woudenberg
NIKHEF and University of Amsterdam, Netherlands [i]

D. Acosta, B. Bylsma, L.S. Durkin, K. Honscheid, C. Li, T.Y. Ling, K.W. McLean, W.N. Murray, I.H. Park,
T.A. Romanowski[21], R. Seidlein
Ohio State University, Physics Department, Columbus, Ohio, USA [p]

D. Bailey, G.A. Blair[22], A. Byrne, R.J. Cashmore, A.M. Cooper-Sarkar, R.C.E. Devenish, N. Harnew, T. Khatri[23],
P. Luffman, P. Morawitz, J. Nash[24], N.C. Roocroft[25], H. Uijterwaal, R. Walczak, F.F. Wilson, T. Yip
Department of Physics, University of Oxford, Oxford, U.K. [o]

G. Abbiendi, A. Bertolin, R. Brugnera, R. Carlin, F. Dal Corso, M. De Giorgi, U. Dosselli,
F. Gasparini, S. Limentani, M. Morandin, M. Posocco, L. Stanco, R. Stroili, C. Voci
Dipartimento di Fisica dell' Universita and INFN, Padova, Italy [f]

J. Bulmahn, J.M. Butterworth, R.G. Feild, B.Y. Oh, J.J. Whitmore[26]
Pennsylvania State University, Dept. of Physics, University Park, PA, USA [q]

G. D'Agostini, M. Guida[27], M. Iori, S.M. Mari, G. Marini, M. Mattioli, A. Nigro
Dipartimento di Fisica, Univ. 'La Sapienza' and INFN, Rome, Italy [f]

J.C. Hart, N.A. McCubbin, K. Prytz, T.P. Shah, T.L. Short
Rutherford Appleton Laboratory, Chilton, Didcot, Oxon, U.K. [o]

E. Barberis, N. Cartiglia, C. Heusch, M. Van Hook, B. Hubbard, W. Lockman, H.F.-W. Sadrozinski, A. Seiden, D. Zer-Zion
University of California, Santa Cruz, CA, USA [p]

J. Biltzinger, R.J. Seifert, A.H. Walenta, G. Zech
Fachbereich Physik der Universität-Gesamthochschule Siegen, Federal Republic of Germany [c]

H. Abramowicz, S. Dagan[28], A. Levy[28]
School of Physics, Tel-Aviv University, Tel Aviv, Israel [e]

T. Hasegawa, M. Hazumi, T. Ishii, M. Kuze, S. Mine, Y. Nagasawa, T. Nagira, M. Nakao, I. Suzuki, K. Tokushuku, S. Yamada, Y. Yamazaki
Institute for Nuclear Study, University of Tokyo, Tokyo, Japan [g]

M. Chiba, R. Hamatsu, T. Hirose, K. Homma, S. Kitamura, S. Nagayama, Y. Nakamitsu
Tokyo Metropolitan University, Dept. of Physics, Tokyo, Japan [g]

R. Cirio, M. Costa, M.I. Ferrero, L. Lamberti, S. Maselli, C. Peroni, R. Sacchi, A. Solano, A. Staiano
Universita di Torino, Dipartimento di Fisica Sperimentale and INFN, Torino, Italy [f]

M. Dardo
II Faculty of Sciences, Torino University and INFN - Alessandria, Italy [f]

D.C. Bailey, D. Bandyopadhyay, F. Benard, S. Bhadra[29], M. Brkic, M.B. Crombie, D.M. Gingrich[30], G.F. Hartner, G.M. Levman, J.F. Martin, R.S. Orr, C.R. Sampson, R.J. Teuscher
University of Toronto, Dept. of Physics, Toronto, Ont., Canada [a]

F.W. Bullock, C.D. Catterall, J.C. Giddings, T.W. Jones, A.M. Khan, J.B. Lane, P.L. Makkar, D. Shaw, J. Shulman
University College London, Physics and Astronomy Dept., London, U.K. [o]

K. Blankenship, J. Kochocki, B. Lu, L.W. Mo
Virginia Polytechnic Inst. and State University, Physics Dept., Blacksburg, VA, USA [q]

K. Charchuła, J. Ciborowski, J. Gajewski, G. Grzelak, M. Kasprzak, M. Krzyżanowski, K. Muchorowski, R.J. Nowak, J.M. Pawlak, T. Tymieniecka, A.K. Wróblewski, J.A. Zakrzewski, A.F. Żarnecki
Warsaw University, Institute of Experimental Physics, Warsaw, Poland [j]

M. Adamus
Institute for Nuclear Studies, Warsaw, Poland [j]

Y. Eisenberg[28], C. Glasman, U. Karshon[28], D. Revel[28], A. Shapira
Weizmann Institute, Nuclear Physics Dept., Rehovot, Israel [d]

I. Ali, B. Behrens, S. Dasu, C. Fordham, C. Foudas, A. Goussiou, R.J. Loveless, D.D. Reeder, S. Silverstein, W.H. Smith
University of Wisconsin, Dept. of Physics, Madison, WI, USA [p]

W.R. Frisken, K.M. Furutani, Y. Iga
York University, Dept. of Physics, North York, Ont., Canada [a]

[1] supported by Worldlab, Lausanne, Switzerland
[2] also at IROE Florence, Italy
[3] now at Univ. of Pisa, Italy
[4] now a self-employed consultant
[5] now at Rutherford Appleton Laboratory
[6] on leave from Jagellonian University, Cracow
[7] supported by the European Community
[8] now at Blohm & Voss, Hamburg
[9] now at DESY
[10] now with Herfurth GmbH, Hamburg
[11] now at CERN
[12] now at Institute for Cosmic Ray Research, University of Tokyo
[13] now with Messrs. Adobe, Santa Clara, CA
[14] now with Messrs. TLC GmbH, Wiesbaden
[15] on leave of absence at DESY, supported by DGICYT
[16] partially supported by Comunidad Autónoma de Madrid, Spain
[17] supported by Fundación Banco Exterior
[18] now at Univ. of California, Davis, CA
[19] now at MIT, Cambridge, MA
[20] now at Fermilab., Batavia, IL
[21] now at Department of Energy, Washington
[22] now at RHBNC, Univ. of London, England
[23] now with A.T. Kearney Ltd., London, England
[24] now with Tessella Support Services, Abingdon, England
[25] now with Arthur Andersen Consultants, London, England
[26] on leave and supported by DESY 1993-94
[27] now at Dip. di Fisica, Univ. di Salerno, Italy
[28] supported by a MINERVA Fellowship
[29] now at York Univ. and DESY
[30] now at Centre for Subatomic Research, Univ.of Alberta, Canada and TRIUMF, Vancouver, Canada

[a] supported by the Natural Sciences and Engineering Research Council of Canada
[b] supported by the FCAR of Quebec, Canada
[c] supported by the German Federal Ministry for Research and Technology (BMFT)
[d] supported by the MINERVA Gesellschaft für Forschung GmbH, and by the Israel Academy of Science
[e] supported by the Israel Ministry of Energy, and by the German Israeli Foundation
[f] supported by the Italian National Institute for Nuclear Physics (INFN)
[g] supported by the Japanese Ministry of Education, Science and Culture (the Monbusho) and its grants for Scientific Research
[h] supported by the Korean Ministry of Education and Korea Science and Engineering Foundation
[i] supported by the Netherlands Foundation for Research on Matter (FOM)
[j] supported by the Polish State Committee for Scientific Research (grant No. 204209101)
[k] supported by the Polish State Committee for Scientific Research (grant No. PB 861/2/91 and No. 2 2372 9102, grant No. PB 2 2376 9102 and No. PB 2 0092 9101)
[l] partially supported by the German Federal Ministry for Research and Technology (BMFT)
[m] supported by the German Federal Ministry for Research and Technology (BMFT), the Volkswagen Foundation, and the Deutsche Forschungsgemeinschaft
[n] supported by the Spanish Ministry of Education and Science through funds provided by CICYT
[o] supported by the UK Science and Engineering Research Council
[p] supported by the US Department of Energy
[q] supported by the US National Science Foundation

1 Introduction

The total photoproduction cross section has been measured recently at HERA by the ZEUS collaboration [1], $\sigma_{tot}^{\gamma p} = 154 \pm 16(\text{stat.}) \pm 32(\text{syst.})$ μb, and by the H1 collaboration [2], $\sigma_{tot}^{\gamma p} = 156 \pm 2(\text{stat.}) \pm 18(\text{syst.})$ μb. Both measurements were obtained at a γp center of mass energy of about $W_{\gamma p} = 200$ GeV, an order of magnitude higher than that of earlier total photoproduction cross section measurements [3]. The H1 and ZEUS measurements are consistent with models predicting a moderate rise of the cross section with energy [4, 5], as observed in $p\bar{p}$ collisions [6].

The first ZEUS measurement was based on 97 events. This paper is based on 5731 events collected in Fall 1992, which allow the determination of the abundances of the various photoproduction processes at HERA energies. The abundances were assumed in the previous paper. This, together with an improved luminosity determination and a better understanding of the photon tagging efficiency, results in a total cross section measurement with a 12% uncertainty. In addition, the calculated radiative corrections have been verified experimentally and taken into account in the total cross section determination.

2 Photoproduction at HERA

2.1 Tagged Photoproduction at HERA

The total photoproduction cross section $\sigma_{tot}^{\gamma p}$ is measured using the interactions of quasi-real photons on protons in the reaction

$$ep \rightarrow e + \gamma^* p \rightarrow e + X.$$

The scattered electron e is measured in the small angle electron calorimeter of the ZEUS luminosity detector and the system X in the central ZEUS detector. The $\gamma^* p$ cross section is related to the electron proton cross section by:

$$\frac{d^2\sigma_{ep}}{dydQ^2} = \frac{\alpha}{2\pi} \cdot \frac{1}{Q^2} \cdot \left[\left(\frac{1+(1-y)^2}{y} - \frac{2(1-y)}{y} \cdot \frac{Q^2_{min}}{Q^2} \right) \cdot \sigma_T^{\gamma^* p}(y, Q^2) + \frac{2(1-y)}{y} \cdot \sigma_L^{\gamma^* p}(y, Q^2) \right].$$

To a very good approximation the kinematic quantities can be obtained from the electron beam energy E_e, the angle between the scattered electron and the beam electron ϑ and the energy of the scattered electron E'_e by:

$$y = 1 - \frac{E'_e}{E_e},$$
$$Q^2 = E_e E'_e \vartheta^2,$$
$$Q^2_{min} = m_e^2 \frac{y^2}{(1-y)}.$$

$\sigma_T^{\gamma^* p}(y,Q^2)$ and $\sigma_L^{\gamma^* p}(y,Q^2)$ are the cross sections for transversely and longitudinally polarized virtual photons respectively. In the kinematic region accepted by the small angle electron calorimeter, the virtual photons are quasi-real with $\sigma_L^{\gamma^* p}(y,Q^2) = 0$ and $\sigma_T^{\gamma^* p}(y,Q^2) = \sigma_{tot}^{\gamma p}(W_{\gamma p})$ at the γp center of mass energy $W_{\gamma p} = \sqrt{4yE_eE_p}$ [4, 7]. Integrating over Q^2 up to the maximum experimentally accepted value Q^2_{max}, gives

$$\frac{d\sigma_{ep}}{dy} = \frac{\alpha}{2\pi}\left[\frac{1+(1-y)^2}{y}\cdot\ln\left(\frac{Q^2_{max}}{Q^2_{min}}\right) - \frac{2(1-y)}{y}\cdot\left(1-\frac{Q^2_{min}}{Q^2_{max}}\right)\right]\cdot\sigma_{tot}^{\gamma p}(W_{\gamma p}).$$

Ignoring the second term in the square brackets yields the Weizsäcker-Williams approximation [8] which, for the present experimental situation, overestimates the flux of photons by approximately 7% [9].

2.2 Classification of Photoproduction Reactions

Studies of hadronic final states in γp reactions at lower energies have led to the phenomenological description by the Vector Dominance Model (VDM) [10, 11] in which the photon first couples to a virtual vector meson (ρ^0, ω, ϕ), which then interacts with the proton. The produced hadronic final state is then very similar to that of hadron-hadron (e.g. πp) collisions.

At higher energies we also expect the same event classes as observed in hadron-hadron interactions [12] to dominate in photoproduction. As in hadronic interactions, we distinguish diffractive and non-diffractive reactions.

For the diffractive reactions we use the following nomenclature:

- elastic vector meson production $\gamma p \to Vp$, where $V = \rho^0, \omega, \phi$ are the low mass vector mesons. The truly elastic Compton scattering $\gamma p \to \gamma p$ has a cross section expected to be about two orders of magnitude smaller and is neglected in the following,
- single diffraction of the proton $\gamma p \to VX$,
- single diffraction of the photon $\gamma p \to Xp$, where X also includes the high mass vector mesons,
- double diffraction $\gamma p \to X_1 X_2$.

The last three process types are later refered to as inelastic diffraction. We call non-diffractive, $\gamma p \to X$, all processes not belonging to one of the above reactions.

In the γp interactions described above, the constituents of the photon can interact with the constituents of the proton (resolved photon interaction) or the photon can couple directly to the partons of the proton (direct photon interaction) [13, 14, 15].

3 Experimental Conditions

3.1 HERA

During 1992, HERA was operated at a proton energy of 820 GeV and an electron energy of 26.7 GeV. There were typically nine colliding electron–proton bunches stored in HERA, as well as an additional proton bunch without a colliding partner and an additional electron bunch without a colliding partner. These additional bunches are called pilot bunches and are used for background studies and the luminosity determination. Typical bunch currents were 0.2 mA for both electron and proton bunches. Lifetimes were usually above 20 hours for the proton beam and about 4 hours for the electron beam. At the ZEUS interaction point (ZEUS-IP) the gas pressure was about $1 \cdot 10^{-9}$ mbar. During the Fall 1992 running, typical luminosities were $5 \cdot 10^{28}$ cm^{-2} s^{-1}.

As the acceptance of the ZEUS detector depends on the vertex position along the beams, the timing and the longitudinal spread of both beams have been monitored using a set of scintillation counters (C5-Counter), upstream of the detector in the direction from which the protons come, which detected stray particles from both beams. The length of the interaction region, which is dominated by the length of the proton bunches, was about $\sigma = 22.5$ cm. Run by run fluctuations of the mean vertex position were ± 5 cm, and the mean vertex position for all runs was displaced by 6 cm from the nominal ZEUS-IP in the electron beam direction.

3.2 ZEUS Detector

The individual components of the ZEUS detector are described in [16]. Here we give only a short description of the components relevant to the present analysis. Throughout this paper we use the standard ZEUS right-handed coordinate system, in which X = Y = Z = 0 is the nominal ZEUS-IP, the positive Z–axis points in the direction of flight of the protons and Y points upwards.

The high resolution uranium-scintillator calorimeter *CAL* [17] consists of forward (FCAL), barrel (BCAL) and rear (RCAL) parts covering polar angles from $\theta_{FCAL} = 2.6°$ to 36.7°, $\theta_{BCAL} = 36.7°$ to 129.1°, and $\theta_{RCAL} = 129.1°$ to 176.2°. Longitudinally it is subdivided into an electromagnetic section (EMC), about 25 X_0 deep, and one (in RCAL) or two (in FCAL and BCAL) hadronic sections (HAC). Under test beam conditions it has an energy resolution of $\sigma_E/E = 0.18/\sqrt{E(\mathrm{GeV})}$ for electrons and $\sigma_E/E = 0.35/\sqrt{E(\mathrm{GeV})}$ for hadrons. Its performance, energy and time calibration are continuously monitored using pedestal triggers, charge and light injection and the signal from the uranium radioactivity. The main features relevant to the present analysis are the sub-nanosecond time resolution for rejection of beam gas events via vertex reconstruction and the low noise of approximately 15 MeV for electromagnetic and 25 MeV for hadronic readout channels.

The central tracking detector *CTD* [18] is a cylindrical drift chamber with 72 layers. During the 1992 data taking it was only partially equipped with read-out electronics (Z–by–timing). Thus its performance was limited to a point resolution of 4 cm in Z and 0.1 cm in (r, ϕ), giving a spatial resolution of $\sigma_Z = 2$ cm and $\sigma_X = \sigma_Y = 0.6$ cm at the ZEUS-IP. For the present analysis

it has been used to reject cosmic muons and to confirm the proper vertex reconstruction from the calorimeter for events with more than two reconstructed tracks.

The *Veto Wall* consists of two planes of orthogonal scintillator strips. The planes have total dimensions of 500 cm $\times$ 600 cm, are separated by 87 cm of iron and are positioned at Z = –727 cm. It is used to recognize proton-gas interactions upstream of the ZEUS detector.

The *C5-Counter* is an assembly of four scintillation counters arranged in two planes around the HERA beam pipe, separated by 0.3 cm of lead at Z = –315 cm. It records separately the arrival times of particles associated with the proton and electron bunches and is used to reject events due to upstream proton-gas interactions.

The *Luminosity Detector* [19] consists of a photon calorimeter and an electron calorimeter. Both are lead-scintillator sandwich calorimeters (5.7 mm Pb–plates and 2.6 mm SCSN–38 scintillator plates) read out by lucite wavelength shifter plates and photomultipliers on two sides. The energy resolutions of both calorimeters are $\sigma_E/E = 0.18/\sqrt{E(\mathrm{GeV})}$, the uniformity in the fiducial volume is within 1% and the non-linearity of response measured in a test beam in the energy range between 1 and 6 GeV is below 1% [20]. The performance of the calorimeters is continuously monitored via pedestal runs, charge and light injections as well as high statistics data from the electron proton bremsstrahlung reaction.

The photon calorimeter is positioned at Z = –107 m. Photons produced at the ZEUS-IP with angles below 0.5 mrad with respect to the electron beam direction leave the vacuum pipe of HERA through a $0.1X_0$ Cu–Be window at Z = –92 m, pass through a $1X_0$ carbon absorber at Z = –103 m and a $1X_0$ Pb absorber just in front of the photon calorimeter. In this way the energy deposited in the calorimeter by synchrotron radiation is negligible. At a depth of $7X_0$ a position detector is installed. It consists of two layers of orthogonal strips of 1 cm wide scintillators read out via silicon photodiodes. The position accuracy for electromagnetic showers above 5 GeV is better than 0.3 cm.

The electron calorimeter is positioned at $Z = -35$ m and accepts electrons in the energy range between 7 and 20 GeV produced at angles up to about 5 mrad with respect to the electron beam direction.

3.3 Trigger

To cope with the high rate of background events, ZEUS has a three level trigger system [16]. The events for the present analysis come from the first level "tagged photoproduction trigger", which required the coincidence of:

- more than 5 GeV energy deposited in the electron calorimeter of the luminosity detector,
- an energy deposit in any of the CAL parts (FCAL, BCAL, RCAL); in the RCAL, where most of the triggers occurred, more than 0.4 GeV in any electromagnetic trigger tower or more than 1.0 GeV in any hadronic trigger tower (more than 2.5 GeV in the towers around the beam pipe) was required. The thresholds for the BCAL trigger towers were 1.0 GeV (for most of the running) and 50(70), 20(25), 10(10) GeV for the EMC(HAC) FCAL trigger towers at radial distances ρ from the beam of: $\rho < 50$ cm, 50 cm$< \rho <$ 130 cm and 130 cm$< \rho$.

The rate of the tagged photoproduction trigger was 5 Hz for a peak luminosity of $2{\cdot}10^{29}\,\mathrm{cm}^{-2}\,\mathrm{s}^{-1}$. At the second level trigger, events with calorimeter timing compatible with upstream interactions were rejected. At the third level trigger, events due to photomultiplier discharges were rejected and tighter timing rejection was applied.

4 Luminosity Determination and Event Selection

4.1 Luminosity Measurement

The luminosity measurement [19] uses the Bethe-Heitler process $ep \to e\gamma p$. Experience from the first running in Summer 1992 resulted in changes in the luminosity measurement [20]. It turned out that the background in the photon calorimeter due to proton halo and other sources was negligible and that the coincidence between the electron and the photon calorimeter was not required for a clean identification of the Bethe-Heitler process. This significantly simplifies the understanding of the acceptance. On the other hand, low energy electromagnetic background caused the veto rate of the Cherenkov counter in front of the photon calorimeter – installed in the original setup to select a sample of non-interacting photons – to fluctuate from run to run. Therefore the Cherenkov counter was removed for the Fall 1992 running.

4.1.1 Measurement of Photon and Electron Energies

The Bethe-Heitler bremsstrahlung process on the beam protons and on the residual gas has been used to calibrate and to determine the acceptances of the two calorimeters of the luminosity detector [20].

Fig. 1 shows the spectrum of bremsstrahlung photons from $ep \to e\gamma p$. The characteristic cut-off at the value of the electron beam energy E_e is clearly visible. The spectrum is well described by a detailed Monte Carlo simulation, which includes the material along the photon path and the resolution of the calorimeter. The calibration of the photon calorimeter is obtained from a fit to the photon spectrum for energies above 18 GeV. The sharpness of the cut-off at a photon energy equal to the electron beam energy E_e is used to verify the energy resolution.

The calibration of the electron calorimeter is obtained by requiring the sum of photon and electron energies to be equal to the HERA electron energy. Fig. 2 shows a scatter plot of electron versus photon energy where this correlation is clearly visible. For a further discussion of this figure we refer to section 5.4. One uncertainty in the calibration of the electron calorimeter is due to possible non-linearities of the photon energy measurement. The non-linearity due to the absorbers in front of the photon calorimeter has been studied via Monte Carlo and taken into account. The non-linearity of the calorimeter has been checked by test beam measurements. The estimated uncertainty is below 2%. Another uncertainty in the calibration at the 2% level is due to gain instabilities of the photomultipliers caused by high event rates and temperature changes. This is taken into account by run to run calibration constants.

4.1.2 Photon Acceptance

Fig. 3 shows, for events from the reaction $ep \to e\gamma p$, a scatter plot of the photon impact points, as measured by the position detector in the photon calorimeter for a particular run, and the calculated aperture limitation due to the HERA beam elements. The width due to the angular spread of the electron beam is 1.4 cm in X and 0.4 cm in Y; the width due to the opening angle of the bremsstrahlung reaction is 0.2 cm and the contribution of the position resolution is also 0.2 cm. The Monte Carlo calculated acceptance, including the effects of absorber material, is 98% for the nominal electron beam angle at the ZEUS-IP. The dependence of the acceptance on the angle of the electron beam has been checked experimentally to an accuracy of 3% by measuring the rate of beam gas bremsstrahlung events for different electron beam angles at the ZEUS-IP [20].

4.1.3 Luminosity Determination

The luminosity is obtained from $R_{ep}(E_\gamma^{th})$, the rate of ep-bremsstrahlung photons above an energy threshold E_γ^{th}, and $\sigma_{ep}^{acc}(E_\gamma^{th})$, the corresponding cross section for the bremsstrahlung reaction corrected for the detector acceptance and resolution,

$$L = \frac{R_{ep}(E_\gamma^{th})}{\sigma_{ep}^{acc}(E_\gamma^{th})}.$$

We use a value E_γ^{th} equal to 5 GeV for the luminosity determination. The cross section of the reaction $ep \to e\gamma p$ is well known [21] and uncertainties, including effects from the finite sizes of the HERA beams, are well below 1% [22].

The only significant background to the reaction $ep \to e\gamma p$ is the beam gas bremsstrahlung reaction $eA \to e\gamma A$, which has the same experimental signature and a similar photon spectrum. The rate of background events R_{eA} is given by $R_{eA} = R_{pilot} \cdot I_{tot}^e / I_{pilot}^e$, where R_{pilot} is the rate from the electron pilot bunch, I_{tot}^e the total electron beam current and I_{pilot}^e the current in the pilot bunch. The background subtracted rate needed for the luminosity determination is $R_{ep} = R_{tot} - R_{eA}$ where R_{tot} is the total bremsstrahlung rate. During the Fall 1992 running R_{eA}/R_{ep} was typically 0.3.

An analysis of runs with more than one pilot bunch in the machine, as well as the measurement of the ratio of beam gas bremsstrahlung rate and bunch current for runs with only electron bunches in HERA, indicates systematic bunch-to-bunch uncertainties of up to 5% in the ratio I_{tot}^e / I_{pilot}^e. This results in an uncertainty of the luminosity of 2%.

The geometric acceptance of the photon calorimeter has been discussed in the previous section. After removing runs in which the electron beam angle at the ZEUS-IP deviated by more than 0.15 mrad from the average direction, the acceptance is then $97 \pm 2\%$.

The accepted cross section $\sigma_{ep}^{acc}(E_\gamma^{th})$ is a function of the effective threshold of the photon calorimeter. From the calibration method, gain stability during data taking, measurements in test beams and Monte Carlo calculations, we estimate the luminosity uncertainty due to the energy scale and the energy resolution function to be below 2.5%.

For the electron and proton bunch currents in the Fall 1992 run, the influence of accidental overlap of several bremsstrahlung events was found to be below 1%. No correction was applied for this effect, but a 1% systematic error has been assigned.

Energy calibration, accidental overlap and other pile-up effects have been continuously monitored by counting $R_{ep}(10\ \mathrm{GeV})$ in addition to $R_{ep}(5\ \mathrm{GeV})$. The distribution of the ratio

$$\frac{R_{ep}(10\ \mathrm{GeV})}{R_{ep}(5\ \mathrm{GeV})} \Big/ \frac{\sigma_{ep}^{acc}(10\ \mathrm{GeV})}{\sigma_{ep}^{acc}(5\ \mathrm{GeV})}$$

for all runs used in the analysis has a mean of 0.998 ± 0.001 and a standard deviation of 0.009.

Whereas the acceptance of the luminosity detectors for measuring the reaction $ep \to e\gamma p$ does not depend on the exact longitudinal vertex position, the acceptance of the central ZEUS detector for photoproduction events does. Using the C5-Counter, evidence for electron satellite bunches, following the main bunches by 8 ns, has been found. Fig. 4 shows a C5 time spectrum. The average fraction of electrons in the satellite bunches was 12%. The satellite bunches collide with the proton bunches 120 cm away from the ZEUS-IP, where, due to increased transverse beam sizes, the luminosity for given electron and proton currents is 52% of the luminosity at the ZEUS-IP. This results in a $6.6 \pm 1.5\%$ correction of the luminosity, as events from satellite bunches are removed in the analysis.

To monitor the proper functioning of the luminosity scalers and the correct treatment of the dead time effects, all rates have been counted in several redundant ways. From the differences we obtain a maximum uncertainty of 0.5% for these effects.

Table 1 summarizes the different effects entering in the systematic uncertainty of the luminosity measurement. Adding all the errors in quadrature results in a luminosity uncertainty of 4.3% for the data analysed in this paper.

4.2 Event Selection and Background Subtraction

A total of $4.21 \cdot 10^6$ events for a total integrated luminosity of about 28 nb^{-1} were recorded.

Runs were used in which the following conditions were fulfilled:

- tagged photoproduction trigger,
- proper adjustment of electron and proton beams,
- high statistics recording of the scatter plot of energy in the photon calorimeter versus energy in the electron calorimeter of the luminosity detector for random bunch crossings (see below),
- proper operation of all detector components required for the analysis,

The resulting data correspond to an integrated luminosity of 12.7 ± 0.6 nb^{-1} after correction for satellite bunches. The main cause for the reduction in luminosity is due to the third requirement listed above. In the process of the analysis approximately $1.8 \pm 0.2\%$ of the events taken have been lost due to reconstruction losses, event corruption and other technical problems.

The following further requirements were imposed to obtain the off-line photoproduction sample which includes identified background events for statistical subtraction:

- more than 5 GeV energy deposited in the electron calorimeter of the luminosity detector (for the final analysis the electron energy is required to be in the range 15.2 GeV to 18.2 GeV),
- more than 0.7 GeV energy deposited in the RCAL,
- a time measured by the RCAL within ± 6.4 ns of the nominal arrival time for ep interactions and, for events with energy deposited in the FCAL, a time difference between FCAL and RCAL within ± 6.4 ns of the nominal value; this cut rejects accidental coincidences between proton beam gas events with electron bremsstrahlung events, electron beam gas events and events from satellite bunches,
- rejection of events with a reconstructed cosmic ray muon,
- statistical subtraction of electron beam gas events,
- statistical subtraction of accidental coincidences of electron bremsstrahlung events with energy deposited in the uranium-scintillator calorimeter (mainly proton gas events),
- less than 1 GeV energy deposited in the photon calorimeter of the luminosity detector to reject radiative photoproduction events and accidental coincidences of proton beam gas with electron bremsstrahlung events.

The losses of good physics events due to the rejection of cosmic ray events and the calorimeter timing cuts have been estimated to be $1.0 \pm 0.3\%$. The cut of 1 GeV in the photon calorimeter of the luminosity detector removes $2.6 \pm 0.8\%$ of the photoproduction events due to an accidental concidence with a bremsstrahlung event. This cut also removes photoproduction events with QED radiation. The resulting radiative correction, which is discussed in more detail in section 5.4, reduces the measured cross section by $1.8 \pm 0.5\%$. In $0.3 \pm 0.2\%$ of the photoproduction events a superimposed accidental bremsstrahlung event deposits sufficient additional energy in the electron calorimeter that the event is removed from the tagged photoproduction sample used in the final analysis.

The statistical subtraction of electron-beam gas background is done in the following way: a sample of such events is obtained from the electron pilot bunches and is added to the data sample with a negative weight, given by the ratio of the electron current in all bunches to the electron current in the pilot bunch. This background is only $0.4 \pm 0.3\%$ for non-diffractive photoproduction events which deposit significant energy in the FCAL; it is however $19.8 \pm 4.3\%$ for the photoproduction events which deposit less than 1 GeV in the FCAL. The subtraction procedure has been checked by comparing the Z–vertex distribution of the background subtracted data sample with the Z–vertex distribution obtained from the C5-Counter [9].

The statistical subtraction of accidental coincidence events is done in the following way: a sample of accidental coincidences of proton gas or other background events in the ZEUS detector with electron bremsstrahlung events is identified by an energy sum measured in the photon and electron calorimeters of the luminosity detector compatible with the electron beam energy in addition to activity in the ZEUS central detector. The continuously recorded scatter plot of photon energy versus electron energy for random bunch crossings, such as that shown in Fig. 2, allows us to determine, as a function of the electron energy E'_e, the fraction of events $f_{e\gamma}(E'_e)$ for which the photon is recorded. The accidental coincidence events are statistically subtracted by adding the recognized accidental events with the weight $-1/f_{e\gamma}(E'_e)$ to the data sample. This removes 1.2±0.2% of the photoproduction events. The success of this method is demonstrated by applying it to a sample of proton gas background events tagged by timing in the C5-Counter or the Veto Wall. As expected, after subtraction all distributions for these events are compatible with zero [9].

Tables 2 and 3 summarize the information on event losses and background subtraction. Fig. 5 shows the electron energy spectrum for the selected photoproduction sample. For the final physics analysis 5731±92 events in the electron energy range from 15.2 GeV to 18.2 GeV have been selected. This cut gives a good compromise between the uncertainty of the photon tagging efficiency and the statistics of the data sample. The cut corresponds to γp center of mass energies $W_{\gamma p}$ between 167 GeV and 194 GeV.

5 General Event Characteristics and Analysis Method

The photoproduction sample selected covers the γp center of mass energy $W_{\gamma p}$ between 167 and 194 GeV, corresponding to a mean energy of the tagged photons of 10 GeV. The Q^2 range is between $Q^2_{min} = 4 \cdot 10^{-8}$ GeV^2 and $Q^2_{max} = 0.02$ GeV^2, with an average of $6 \cdot 10^{-4}$ GeV^2. Due to the large momentum imbalance between photon and proton, the acceptance of the ZEUS detector is very asymmetric in the γp center of mass system. For $W_{\gamma p} = 180$ GeV the center of mass angle $\theta^* = 90°$ corresponds to a pseudorapidity $\eta = 2.2$ and to a polar angle $\theta = 12.5°$ in the HERA system. The ZEUS uranium-scintillator calorimeter covers the range θ^* from 23° to 179.6°.

We use the following strategy to obtain the acceptances of the different reactions contributing to photoproduction, their fractional cross sections and finally the total cross section:

- the acceptances of the photon tagging and of the main detector are treated separately which is a good assumption if the cross sections of the individual subprocesses and the corresponding acceptances do not vary significantly in the $W_{\gamma p}$ interval considered,
- for the acceptance of the hadronic system in the uranium-scintillator calorimeter we use a variety of models to generate Monte Carlo event samples, pass them through the ZEUS simulation and analysis program chain and compare them to the measured data sample. The agreement between experimental data and Monte Carlo sample for the different models and model parameters allows us to determine the fractional cross sections and acceptances compatible with the experimental data and finally the acceptance-corrected number of events,

- the acceptance of the photon tagging is obtained from a Monte Carlo calculation, which is cross checked by high statistics data from the reaction $ep \to e\gamma p$,
- radiative corrections are taken from a Monte Carlo study, which is checked against experimental data,
- combining the corrected number of events with the photon flux for the given luminosity gives the total and partial photoproduction cross sections.

5.1 Monte Carlo Models for Photoproduction

Models based on hadron-hadron physics were used to simulate the different photoproduction reactions discussed in section 2.2. The models were adapted either by replacing the structure function of one of the hadrons by the photon structure function, which is an option in PYTHIA [23], or by superposing π^+ and π^- proton interactions (HERWIG [24] minimum bias events).

Non-diffractive events were simulated using three classes of models:

- models based on parametrizations of multiplicity and p_t distributions, without any dynamical ansatz; an example is the minimum bias hadron-hadron generator in HERWIG. We use for the corresponding Monte Carlo sample the nomenclature

  $$f_{herlow} * herlow,$$

  where f stands for the unknown fraction of this subprocess in the data sample and $herlow$ for the distribution of the minimum bias hadron-hadron events, parametrized in HERWIG using a cylindrical phase space and a multiplicity distribution chosen to describe the multiplicity distribution measured by the uranium-scintillator calorimeter.
- models with phenomenological QCD parton dynamics like the PYTHIA minimum bias generator,

  $$f_{pytlow} * pytlow,$$

  where $pytlow$ are semihard minimum bias events from PYTHIA with QCD cross sections regularized at low p_t, which includes several parton-parton interactions per γp interaction; this model is closely related to total cross section models based on the sum of a soft and a minijet component with eikonalization [25, 26].
- models, which simulate γp interactions as the sum of a non-perturbative soft component and a perturbative QCD minijet component [25],

  $$f_{soft} * soft + f_{hard} * hard.$$

  For *soft* we have used the soft PYTHIA two string model with a mean transverse momentum of the charged particles at the generator level of 0.28 GeV, 0.33 GeV and 0.41 GeV (*soft0.28, soft0.33, soft0.41*). For *hard* we have used the perturbative, resolved photon process with a lower transverse momentum cutoff p_t^{min}. We have used PYTHIA with

p_t^{min} = 1.8 GeV and 2.0 GeV (*pyt1.8, pyt2.0*), as well as HERWIG with p_t^{min} = 1.5 GeV, 1.7 GeV and 2.0 GeV (*her1.5, her1.7, her2.0*). For the parton distribution function in the proton we have used the defaults of PYTHIA and HERWIG extrapolated into the low x region, and for the parton distribution function in the photon we have used the parametrization of Drees and Grassie [27]. The energy distributions measured in the detector are not very sensitive to the choice of the parton distribution functions.

The four classes of diffractive reactions were generated in the following ways:

- elastic vector mesons $\gamma p \to Vp$ using PYTHIA and HERWIG; with relative fractions of ρ^0, ω and ϕ mesons of $1/2.2 : 1/18.4 : 1/23.6$, as given by the vector meson-photon couplings $(f_V^2/4\pi)^{-1}$ [11],
- single diffraction of the proton $\gamma p \to VX$ using PYTHIA,
- single diffraction of the photon $\gamma p \to Xp$ using PYTHIA, a modified version of HERWIG and the Nikolaev-Zakharov model [28],
- double diffraction $\gamma p \to X_1 X_2$ using PYTHIA.

The free parameters of the diffractive models are the slope parameter b and the exponent a of the differential cross section $d^2\sigma/dtdM_X^2 \propto e^{bt}/(M_X^2)^a$ to produce a diffractive system of mass M_X with four momentum transfer t, the minimum value of M_X, the maximum value of M_X, and the decay parameters of the M_X system. The value of a has been varied between 1.0 and 1.25. The slope parameter b has been varied in the range from 8 to 16 GeV^{-2} for the elastic reaction and half this value for the inelastic diffraction [29]. For the photon diffraction 1.0 GeV has been used as the minimum value for M_X in PYTHIA and HERWIG and 1.7 GeV in the Nikolaev-Zakharov model. For the proton diffraction a value of 1.14 GeV was used. $M_X^2/W_{\gamma p}^2 = 0.1$ has been used for the maximum value of M_X. For the decay of the systems X the limited p_t string decay from PYTHIA, the Nikolaev-Zakharov model and the isotropic decay from HERWIG were tried. The data ruled out the isotropic decay, so only PYTHIA and the Nikolaev-Zakharov model were finally used.

No direct photon component was used in the event simulation. One might expect that a significant fraction of the direct events could escape the event selection, in particular the $E_{RCAL} > 0.7$ GeV cut, since no photon remnant enters the RCAL. The following argument convinces us that this is not the case. For a p_t^{min} of 2 GeV the events with total transverse energy, E_T, up to 25 GeV have distributions in the global event variables which are practically identical for the resolved and the direct contributions. Only 3% of the measured events have a value of E_T bigger than 25 GeV of which 10–30% [15, 30] are expected to be due to direct processes. Therefore neglecting direct processes in the event simulation affects the cross section determination by less than 1%.

5.2 Analysis of the Hadronic System

Given the number of models and their many adjustable parameters the analysis of the hadronic system is a difficult task. It is somewhat simplified by the observation that, due to the high

center of mass energy, diffractive and non-diffractive photoproduction can be separated without too much overlap. This can be seen from Fig. 6, which shows the distribution of E_{FCAL}, E_{BCAL}, E_{RCAL} and the transverse energy E_T. The data fall into two classes: events with essentially zero energy in FCAL, as expected for elastic and for low mass photon and proton diffractive events, and events in which a significant amount of energy is deposited in FCAL, as expected for non-diffractive events. The corresponding statistics are:

$$E_{FCAL} > 1\text{GeV}; \quad N = 4852 \pm 72 \text{ events},$$
$$E_{FCAL} < 1\text{GeV}; \quad N = 879 \pm 59 \text{ events}.$$

In the further analysis these events will be treated separately.

From the Monte Carlo simulations we find that all elastic events have $E_{FCAL} < 1$ GeV. The E_{FCAL} separation is less clear for inelastic diffraction. The fraction of events with $E_{FCAL} < 1$ GeV depends not only on which particle diffracts (γ diffraction, p diffraction, double diffraction), but also on the diffractive mass spectrum and its decay. If the model parameters are varied in the ranges discussed in section 5.1, the fractions of events in the $E_{FCAL} < 1$ GeV sample vary between 0.5 and 0.7 for photon diffraction, between 0.3 and 0.5 for proton diffraction and between 0.3 and 0.4 for double diffraction.

We should also mention that the data sample used to determine the subprocess fractions and acceptances is bigger than the one used to obtain the total cross section. In order to increase the statistics, the data sample contains in addition the runs for which no statistical background subtraction was possible. For these runs the background was removed using signals in the C5-Counter or the Veto Wall with timing compatible with proton-beam gas interaction upstream of the ZEUS detector.

5.2.1 Data Sample with $E_{FCAL} > 1$ GeV

Based on the discussion of the previous section, the following three Monte Carlo samples were used to describe the data sample $E_{FCAL} > 1$ GeV:

$$f_{herlow} * herlow + f_{diff} * diff,$$

$$f_{pytlow} * pytlow + f_{diff} * diff,$$

$$f_{soft} * soft + f_{hard} * hard + f_{diff} * diff.$$

where the f_i's are the fractions of events of reaction i in the $E_{FCAL} > 1$ GeV sample. Single diffractive events from the PYTHIA program have been used for the small admixture of diffractive events, *diff*.

For each of the models, with the parameters varied in the given range, the fractions f_i have been determined by fits to the distributions of E_{FCAL} and E_{BCAL}, which are essentially uncorrelated.

E_{RCAL} was not used in the fits since its distribution hardly depends on the type of the process. A fit was done by minimizing the following variable

$$\chi^2_{fit} = \frac{1}{(N_{bins} - N_p)} \sum_{E_{FCAL}, E_{BCAL}} \sum_{bins} \frac{(N^{exp} - \sum \alpha_i f_i N_i^{MC})^2}{(N^{exp} + \sum \alpha_i^2 f_i^2 N_i^{MC})}$$

where N^{exp} and N^{MC} are the numbers of the experimental and the Monte Carlo events respectively, N_{bins} is the total number of histogram bins, N_p is the number of fit parameters, f_i is the fraction of subprocess i and α_i is the ratio of the number of events in the experimental data to the number of accepted events in the Monte Carlo sample for subprocess i.

The best value of the mean transverse momentum of charged particles $\langle p_t \rangle_{ch}$ in the soft PYTHIA model was determined to be $\langle p_t \rangle_{ch} = 0.41$ GeV by the comparison of average transverse momenta of condensates in data and Monte Carlo samples. A condensate is defined as a contiguous group of calorimeter cells with a sum of energy of at least 0.1 GeV for a group of only EMC cells and at least 0.2 GeV for any other group of cells. The values of p_t^{min} in the hard PYTHIA model and the hard HERWIG model which describe the data best, were obtained by trying different values and searching for the minimum value of χ^2_{fit}. As an additional cross check it has been verified that the average transverse energy of the calorimeter condensates is well reproduced.

Table 4 summarizes the acceptances for the Monte Carlo samples with $E_{FCAL} > 1$ GeV. They vary between 78% and 95% for the models analyzed. It has been checked that for the $E_{FCAL} > 1$ GeV sample the acceptance depends only weakly on the vertex position. This is demonstrated in Fig. 7a. The measured Z–vertex distribution for the $E_{FCAL} > 1$ GeV data sample, shown in Fig. 7b, has been used as Monte Carlo input for the $E_{FCAL} < 1$ GeV sample where the acceptance does depend strongly on the vertex position.

Table 5 presents the main results of the fits: given are the fractions of the subprocesses f_i, the acceptances and the χ^2-values. In addition to χ^2_{fit}, the χ^2 values for the E_{FCAL}, E_{BCAL}, E_{RCAL} and E_T distributions are given. The best fits of HERWIG and PYTHIA are compared to the data in Figs. 8, 9 and 10. Fig. 10, which shows the individual contributions for the model *pytlow + diff*, demonstrates that the distributions for the non-diffractive and the diffractive component are sufficiently different to well determine the fractions by the fit.

The results of the fits can be summarized:

- the data sample with $E_{FCAL} > 1$ GeV is well described by hadron-hadron minimum bias events (HERWIG, PYTHIA); thus γp reactions have gross features similar to hadron-hadron reactions,
- the models which describe photoproduction as a sum of a soft and a hard component give generally worse fits. The data favor a value of $p_t^{min} = 2$ GeV, and the *hard* component accounts for more than 60% of the data. It should be noted that the so–called *hard* resolved component can actually yield relatively soft events due to the relatively low minimum p_t of 2 GeV. The high fraction of *hard* processes thus does not imply a difference between γp and πp reactions,

- the fits yield the following ranges for the fractions of subprocesses:
  - f_{soft}: 0.16 – 0.32,
  - f_{hard}: 0.62 – 0.73,
  - f_{pytlow}: 0.88 – 0.96,
  - f_{diff}: 0.06 – 0.14, (the fit $herlow + diff$ gives $f_{diff} = 0$, which is consistent with a lower limit of 0.06 for the diffractive fraction, as HERWIG minimum bias events implicitly include diffractive events),
- the acceptance for the $E_{FCAL} > 1$ GeV data sample lies between 0.83 and 0.95.

So far in the analysis step-function energy thresholds in the trigger have been assumed to determine the acceptances. Given the low threshold values, the effects of noise, finite energy steps for the trigger and channel to channel gain variations have to be taken into account. To estimate these effects, in the analysis the energy thresholds have been raised for both data and Monte Carlo samples and the fraction of events lost has been compared. This results in a correction factor for the acceptance of 0.98±0.01 for the non-diffractive sample, 0.97±0.01 for the photon diffractive and double diffractive samples and 0.88±0.06 for the proton diffractive sample.

We obtain the overall acceptance and its uncertainty from the mean value and the range of the acceptance values from Table 5 for the four models that give lowest χ^2_{fit} values, multiplied by the correction factor 0.98 ± 0.01 from the previous paragraph. The resulting acceptance for the $E_{FCAL} > 1$ GeV sample is 0.86 ± 0.07, with an acceptance for the non-diffractive processes of 0.90 ± 0.03 and for the diffractive sample of 0.61 ± 0.06. This results in the following numbers of acceptance corrected events:

- all $E_{FCAL} > 1$ GeV events: $5641 \pm 84 \pm 451$,
- non-diffractive events for $E_{FCAL} > 1$ GeV: $4852 \pm 73 \pm 162 \pm 216$,
- diffractive events for $E_{FCAL} > 1$ GeV: $789 \pm 36 \pm 79 \pm 316$.

The first error is the statistical one, the second is the error due to the acceptance uncertainty and the third one, where applicable, is the error due to the uncertainty of the fraction of diffractive events.

5.2.2 Data Sample with $E_{FCAL} < 1$ GeV

The acceptances for the individual diffractive processes have been calculated by Monte Carlo methods. The results are summarized in Table 6. Due to the strong collimation of the produced particles around the beam direction, the acceptance values strongly depend on the Z-vertex position, as shown in Fig. 11. As input for the Monte Carlo we use the Z-vertex distribution shown in Fig. 7b, as discussed in section 5.2.1.

The acceptances for elastic vector meson production were calculated assuming relative rates for ρ^0, ω and ϕ mesons of $1/2.2 : 1/18.4 : 1/23.6$. The corresponding acceptances are 38%, 21% and 3% for the vertex centered at Z = 0. They were combined to get an overall acceptance for elastic vector meson production of 31 ± 4% as shown in Table 6. The systematic errors

given include the uncertainty of the slope parameter b of the differential cross section, and an uncertainty of ± 5 cm for the mean Z-vertex position.

The final states Vp and VX can be separated from Xp and XX by the radial distribution of the energy in the RCAL. For Vp and VX the energy is deposited close to the beam pipe, whereas it is more evenly distributed for Xp and XX. We define the energy weighted radius in the RCAL ($\theta > 135°$)

$$\langle R_{RCAL} \rangle = \frac{\sum_{cond} r_{cond} \cdot E_{cond}}{\sum_{cond} E_{cond}}.$$

The r_{cond} and E_{cond} refer to the radial distances and energies of the condensates in the RCAL, as defined in the preceding section.

The Monte Carlo distributions of $\langle R_{RCAL} \rangle$ are shown in Fig. 12 for the final states Vp from the PYTHIA and Xp from the Nikolaev-Zakharov model. From factorization arguments we expect VX and Vp to have similar $\langle R_{RCAL} \rangle$ distributions. The same is true for Xp and XX.

A fit to the $\langle R_{RCAL} \rangle$ distribution allows the determination of r, the ratio of the number of vector meson events to diffractive events

$$r = \frac{N_{Vp} + N_{VX}}{N_{Vp} + N_{VX} + N_{Xp} + N_{XX}}.$$

N_{Vp} is the number of elastic events in the data sample, N_{VX} the number of proton diffractive events, N_{Xp} the number of photon diffractive events and N_{XX} the number of double diffractive events. The Nikolaev-Zakharov model for Xp, which describes the data best (Fig. 12), gives a value $r = 0.42 \pm 0.05$; a fit with PYTHIA for Xp, which gives a poorer description, results in $r = 0.36 \pm 0.05$. We take as the final result $r = 0.42 \pm 0.05(\text{stat.}) \pm 0.06(\text{syst.})$.

The estimation of the contributions from elastic and inelastic vector meson production is based on the Monte Carlo study. It is assumed that the cross sections for the single diffractive channels are equal and each of them twice the cross section for the double diffraction - as found in πp data [31] and expected from theoretical parametrizations [32]. This allows us to determine the ratio of N_{Vp} to N_{VX}.

The resulting contributions to the $\mathrm{E}_{FCAL} < 1$ GeV sample are:

$$N_{Vp} = (0.30 \pm 0.08) \cdot N_{EFCAL<1}$$
$$N_{VX} = (0.12 \pm 0.04) \cdot N_{EFCAL<1},$$

where $N_{EFCAL<1}$ is the measured number of events with $E_{FCAL} < 1$ GeV. The error includes the uncertainty from the determination of r and from the models used. The remaining event fraction is due to the sum N_{Xp} plus N_{XX}.

The effect of the shape of the calorimeter energy threshold in the trigger has been studied in the way discussed in the section 5.2.1. The correction factor is 0.97 ± 0.01 for photon diffractive events and 0.88 ± 0.06 for elastic and proton diffractive vector meson production. Combining the reaction fractions with the acceptances gives the following acceptance corrected numbers of events in the $E_{FCAL} < 1$ GeV sample:

- all events: $1941 \pm 170(\text{stat.}) \pm 239(\text{syst.})$,
- elastic vector meson production: $964 \pm 203(\text{stat.}) \pm 326(\text{syst.})$,
- inelastic diffraction: $977 \pm 107(\text{stat.}) \pm 147(\text{syst.})$.

The above numbers lead to the overall acceptance for the $E_{FCAL} < 1$ GeV sample of 0.46 ± 0.08.

5.2.3 Summary on Event Fractions and Acceptances

Combining the results from the two subsections 5.2.1 and 5.2.2 gives the final numbers of events, event fractions and acceptances, shown in Table 7.

5.3 Photon Tagging Efficiency

The photon tagging efficiency for photoproduction events, i.e. the acceptance of the electron calorimeter of the luminosity detector as a function of the energy and angle of the scattered electron, was obtained from Monte Carlo calculations. It depends critically on the precise knowledge of the position and the direction of the electron beam at the ZEUS-IP, of the HERA magnetic elements, of the position of the electron calorimeter and its energy calibration. High statistics data from the bremsstrahlung reaction $ep \to e\gamma p$ with different electron beam tilts up to 0.5 mrad at the ZEUS-IP have been used to find the best parameters and verify the Monte Carlo calculation. The following strategy has been employed [20]: the photon position, measured in the photon calorimeter, gives the angle of the electron beam at the ZEUS-IP. From the difference of beam energy and measured photon energy we obtain the predicted electron energy. The fraction of events with an electron recorded with compatible energy gives the acceptance as a function of the predicted energy. To obtain it as a function of the measured energy, the smearing due to the resolutions for both electron and gamma calorimeter has been taken into account. The comparison of the measured acceptance with the Monte Carlo calculation allows us to adjust the geometric parameters within their known uncertainty. These parameters are then used to calculate the acceptance for photoproduction events.

The photoproduction events are produced in the E'_e range from 9.0 to 22.0 GeV and the Q^2 range from Q^2_{min} to $Q^2_{max} = 0.02$ GeV^2 according to the ALLM parametrization of the proton structure function [4]. Effects of the finite value of the electron mass are included. Fig. 5 shows the comparison between the measured and the generated electron spectra. The agreement is satisfactory. The resulting photon tagging acceptance for E'_e between 15.2 GeV and 18.2 GeV is $77 \pm 7\%$. The error has two main sources: the uncertainty in the energy calibration of the electron calorimeter and the uncertainty in the electron transport through the HERA magnets.

To obtain the error from the uncertainty of the energy calibration (see section 4.1.1) we have scaled the electron energy by $\pm 2\%$ for both data and Monte Carlo sample, which resulted in a $\pm 7\%$ change in the number of events accepted for $15.2 < E'_e < 18.2$ GeV, which we take as an error estimate.

To estimate the error due to the electron transport, in the Monte Carlo study the tilt of the electron beam was varied by ± 0.15 mrad at the ZEUS-IP, the electron beam position by ± 1 mm and the position of the HERA magnets also by ± 1 mm. From the change in the number of Monte Carlo events in the acceptance window, we obtain an uncertainty of 5%. Adding both contributions in quadrature gives an acceptance uncertainty of 9%.

5.4 Radiative Corrections

A Monte Carlo study of radiative corrections to ep scattering at low Q^2 [9], using HERACLES [33] events passed through the ZEUS detector simulation program, expects a 1.8% reduction for the number of measured photoproduction events. This value agrees with a Monte Carlo study for an experimental situation similar to this experiment [34].

In the following we check the magnitude of the radiative corrections using the photon spectrum measured in the photon calorimeter of the luminosity detector. The recorded photon energy spectrum is contaminated by random coincidences of bremsstrahlung events with photoproduction events, which are subtracted using the measured high statistics bremsstrahlung spectrum from random ep bunch crossings [9]. Fig. 13 shows the spectra for photon energies below 5 GeV, normalized to the area up to 5 GeV, for:

- the events of the off-line photoproduction sample, without the $E_\gamma < 1$ GeV photon energy cut (dashed),
- the randomly triggered bunch crossings (dotted),
- difference of the above two spectra (solid), which is the experimental spectrum of radiative photons from photoproduction events.

Above a photon energy of 5 GeV the number of background events is much larger than the number of photoproduction events, which results in large errors after background subtraction.

Below $E_\gamma = 5$ GeV two experimental difficulties should be pointed out. For photons of such low energy, the synchrotron radiation absorber in front of the gamma calorimeter causes a non-linearity of response, which may not be correctly simulated by the Monte Carlo program, and at low energies, the spectrum is sensitive to the exact shape of the pedestal, which is influenced by the high rate in the photon calorimeter. As a result the spectrum below 1.2 GeV is not reliable.

The observed photon energy spectrum and the one obtained from the Monte Carlo study are presented in Fig. 14. Above 1.2 GeV the distributions agree within the experimental errors and corroborate the estimation of the radiative corrections. Monte Carlo results and data agree within 0.5% on the fraction of radiative events in the photon energy interval between 1 and 5 GeV. We thus assign an uncertainty of 0.5% to the 1.8% Monte Carlo estimation for the loss of photoproduction events with respect to the Born cross section (Table 2).

6 Results and Discussion

6.1 Photoproduction Cross Sections

The corrected number of events, presented in Table 7, together with the corrections for the event losses of 5.7%, the measured luminosity of 12.7 nb^{-1} and the photon tagging efficiency of 77% are used to calculate σ_{ep}, the ep cross section for the scattered electron energy range of $15.2 < E'_e < 18.2$ GeV and the range $4 \cdot 10^{-8} < Q^2 < 0.02$ GeV^2. The corresponding γp

center of mass energy range is $167 < W_{\gamma p} < 194$ GeV. The relation between γp and ep cross sections given in section 2.1 yields after integration over the corresponding y and Q^2 range a photon flux factor of $5.82 \cdot 10^{-3}$. After correction by 1.8% for the loss of radiative events total photoproduction cross section for an average $W_{\gamma p}$ of 180 GeV is obtained:

$$\sigma_{tot}^{\gamma p} = 143 \pm 4(\text{stat.}) \pm 17(\text{syst.})\ \mu\text{b}.$$

The statistical error of 3% includes the statistical background subtraction. The systematic error of 12% is the quadratic sum of the uncertainties of 1.0% from the data selection cuts, 4.3% from the luminosity determination, 6.7% from the acceptance of the main detector, 9.0% from the photon tagging efficiency, and 0.5% from the radiative corrections.

The fractions of the different photoproduction cross sections and their errors are given in Table 7. Using the total cross section we obtain for the non-diffractive photoproduction reactions a cross section of

$$\sigma_{nd}^{\gamma p} = 91 \pm 11\ \mu\text{b},$$

for the inelastic diffractive photoproduction reactions

$$\sigma_{d}^{\gamma p} = 33 \pm 8\ \mu\text{b},$$

and for the elastic photoproduction reactions

$$\sigma_{el}^{\gamma p} = 18 \pm 7\ \mu\text{b}.$$

Assuming further that the ρ^0 contributes 82% of the elastic cross section [11], we obtain a cross section for the reaction $\gamma p \to \rho^0 p$ at HERA energies of: $\sigma_{\rho^0 p}^{\gamma p} = 14.8 \pm 5.7\ \mu$b. The errors quoted on the partial cross sections include statistical and systematic errors added in quadrature.

6.2 Discussion

The energy dependence of the total photoproduction cross section is displayed in Fig. 15, which includes the lower energy data above the resonance region ($W_{\gamma p} > 1.75$ GeV) [3] as well as the H1 measurement [2] at HERA energies. Also included is our earlier low statistics measurement [1]. The curves labeled DL [5] and ALLM [4] are parametrizations inspired by Regge–type analyses and describe well the energy behavior of the data. The cross sections calculated with the inclusion of QCD hard scattering (minijets) [25] depend on the parton distributions in the photon and proton, on the value used for p_t^{min}, the minimum value of p_t where perturbative QCD starts to be applicable, and on the value used for the probability of the photon to act like a hadron. The curve labeled as "minijets" is a calculation of QCD hard scattering with a value of $p_t^{min} = 2$ GeV using the Drees–Grassie (DG) parton distributions of the photon [27]. Within the present measurement errors it is also compatible with the data.

In Figure 16 we present a compilation of cross sections [35] measured at lower energies for the reaction $\gamma p \to Vp$, where $V = \rho^0, \omega, \phi$, together with the new measurement of the present experiment. The full curve is a calculation by Schuler and Sjöstrand [32] who use the additive quark model together with VDM to estimate the Vp cross sections, a phenomenological parametrization of the energy dependence of the slopes of the differential cross section of the $\gamma p \to Vp$ reactions, and the optical theorem. As can be seen from the figure, the parametrization agrees well with the new ZEUS measurement. Also the other partial cross sections agree with predictions by these authors.

7 Summary

The ZEUS detector at HERA has been used to measure the total photoproduction cross section at an average center of mass energy of 180 GeV via interactions of 26.7 GeV electrons with 820 GeV protons tagged by an outgoing electron scattered at a small angle with respect to the incoming electron direction. In this study, the scattered electron energy was restricted to $15.2 < E'_e < 18.2$ GeV. Thus the exchanged photon is almost real, with a Q^2 in the range $4 \cdot 10^{-8} < Q^2 < 0.02$ GeV^2, the average being $\langle Q^2 \rangle \approx 6 \times 10^{-4}$ GeV^2. From the measured total ep cross section in this region we obtain the average total γp cross section for the γp center of mass energy of $167 < W_{\gamma p} < 194$ GeV: $\sigma_{tot}^{\gamma p} = 143 \pm 4(\text{stat.}) \pm 17(\text{syst.})\mu$b. This value is in good agreement with parametrizations based on Regge models and also with some minijet-based models, provided a high enough minimum transverse momentum, p_t^{min}, is chosen.

We have also determined cross sections for photoproduction subprocesses. The non-diffractive cross section is $\sigma_{nd}^{\gamma p} = 91 \pm 11\mu$b, the inelastic diffractive dissociation cross section is $\sigma_d^{\gamma p} = 33 \pm 8\mu$b, and the elastic photoproduction cross section of the vector mesons ρ^0, ω, and ϕ is $\sigma_{el}^{\gamma p} = 18 \pm 7\mu$b. For the partial cross sections, the quoted error includes statistical and systematic errors added in quadrature.

Acknowledgements

We thank the DESY Directorate for their strong support and encouragement. The remarkable achievements of the HERA machine group were essential for the successful completion of this work, and are gratefully appreciated.

References

[1] ZEUS Collab., M.Derrick et al., Phys. Lett. **B293** (1992) 465.

[2] H1 Collab., T. Ahmed et al., Phys. Lett. **B299** (1993) 374; M. Erdmann et al., DESY 93-077, presented at the 28th Rencontres de Moriond (20-27 March 1993).

[3] D.O. Caldwell et al., Phys. Rev. Lett. **40** (1978) 1222; S.I.Alekhin et al., CERN–HERA 87–01 (1987).

[4] H. Abramowicz, E.M. Levin, A. Levy and U. Maor, Phys. Lett. **B269** (1991) 465.

[5] A. Donnachie and P.V. Landshoff, Nucl. Phys. **B244** (1984) 322; P.V. Landshoff, Nucl. Phys. B (Proc. Suppl.) **18C** (1990) 211.

[6] Review of Particle Properties, Phys. Rev. **D45** (1992).

[7] A.I. Lebedev, Proc. Workshop on Physics at HERA, DESY (1991) 613.

[8] C.F. von Weizsäcker, Z. Phys. **88** (1934) 612; E.J. Williams, Phys. Rev. **45** (1934) 729.

[9] B. Burow, PhD Thesis (University of Toronto), 1993; DESY F35D-94-01, Jan 1994.

[10] J.J. Sakurai, Ann. Phys. **11** (1960) 1.

[11] T.H. Bauer et al., Rev. Mod. Phys. **50** (1978) 261.

[12] G. Giacomelli, Int. Jour. Mod. Phys. **A Vol.5** (1990) 223; C. Geich-Gimbel, Int. Jour. Mod. Phys. **A Vol.4** (1989) 1527; K. Goulianos, Phys. Rep. **101** (1983) 169.

[13] OMEGA Photon Collab., R.J. Apsimon et al., Z. Phys. **C43** (1989) 63.

[14] NA14 Collab., E. Auge et al., Phys. Lett. **168B** (1986) 163; R. Barate et al., Phys. Lett. **174B** (1986) 458.

[15] ZEUS Collab., M. Derrick et al., DESY 93-151, accepted for publication in Phys.Lett. B.

[16] The ZEUS Detector, Status Report, DESY(1993).

[17] M. Derrick et al., Nucl. Instrum. Methods **A 309** (1991) 77; A. Andresen et al., Nucl. Instrum. Methods **A 309** (1991) 101; A. Bernstein et al., Nucl. Instrum. Methods **A 336** (1993) 23.

[18] N. Harnew et al., Nucl. Instrum. Methods **A 279** (1989) 290; C.B. Brooks et al., Nucl. Instrum. Methods **A 283** (1989) 477; B. Foster et al., Nucl. Phys. B, Proc. Suppl. **B 32** (1993) 181.

[19] D. Kisielewska et al., Fast Luminosity Monitoring at HERA, DESY-HERA report 85-25 (1985), J. Andruszkow et al., DESY 92-066 (1992).

[20] K. Piotrzkowski, PhD Thesis (Cracow, INP-Exp), 1993; DESY-F35D-93-06, Oct 1993.

[21] H.Bethe and W.Heitler, Proc. Roy. Soc., **A146** (1934) 83.

[22] G.L. Kotkin et al., Z. Phys. **C39** (1988) 61.

[23] T. Sjöstrand, Z. Phys. **C42** (1989) 301; H-U. Bengtsson and T. Sjöstrand, Comput. Phys. Commun. **46** (1987) 43.

[24] B.R. Webber, Ann. Rev. Nucl. Part. Sci. **36** (1986) 253; G. Marchesini et al., Comput. Phys. Commun. **67** (1992) 465.

[25] M. Drees and F. Halzen, Phys. Rev. Lett **61** (1988) 275; R. Gandhi and I. Sarcevic, Phys. Rev. **D44** (1991) R10; J.R. Forshaw and J.K. Storrow, Phys. Lett. **B268** (1991) 116; R.S. Fletcher, T.K. Gaisser and F. Halzen, Phys. Rev. **D45** (1992) 377.

[26] T. Sjöstrand and M. Zijl, Phys. Rev. **D36** (1987) 2019.

[27] M. Drees and K. Grassie, Z. Phys. **C28** (1985) 451.

[28] N.N. Nikolaev and B.G. Zakharov, Z. Phys. **C53** (1992) 331; P. Bruni et al.,Proc. Workshop on Physics at HERA, DESY (1991) 363; A. Solano, PhD Thesis (University of Torino), 1993.

[29] T.J. Chapin et al., Phys. Rev. **D31** (1985) 17.

[30] M. Drees and R.M. Godbole, Phys. Rev. **D39** (1989) 169.

[31] T.A. Fuess, PhD Thesis (MIT), September 1987; T.A. Fuess et al., Nucl. Phys. **B414** (1994) 3.

[32] G.A. Schuler and T.Sjöstrand, Phys. Lett. **B300** (1993) 169; G.A. Schuler and T.Sjöstrand, Nucl. Phys. **B407** (1993) 539.

[33] A. Kwiatkowski et al., Comput. Phys. Commun. **69** (1992) 155.

[34] K. Charchula and J. Gajewski, DESY 92-173, (1992), accepted for publication in the Int. Jour. Mod. Phys. A.

[35] "Total Cross-Sections for Reactions of High Energy Particles", Landolt-Börnstein, New Series, Vol. 12b, H. Schopper, Ed. (1987).

Cause	Systematic uncertainty
Cross section	1.0%
Electron gas background subtraction	2.0%
Photon acceptance	2.0%
Calorimeter calibration/resolution	2.5%
Accidental overlaps	1.0%
Satellite bunches	1.5%
Counting errors	0.5%
Total uncertainty	4.3%

Table 1: Systematic effects for the luminosity determination.

Cause	Event fraction	Uncertainty
Reconstruction losses	1.8%	0.2%
Analysis cuts	1.0%	0.3%
Overlay bremsstrahlung-photoproduction	2.9%	0.8%
Total	5.7%	1.0%
Radiative events	1.8%	0.5%

Table 2: Correction factors for event losses.

Cause	Uncertainty
Electron-beam gas background	0.8%
Accidental coincidence bremsstrahlung and background	0.2%
Total	0.8%

Table 3: Error estimation on statistical background subtraction.

Model		Acceptance
PYTHIA	*soft0.28*	0.78
	soft0.33	0.85
	soft0.41	0.89
HERWIG	*herlow*	0.95
PYTHIA	*pytlow*	0.89
PYTHIA	*pyt1.8*	0.90
	pyt2.0	0.90
HERWIG	*her1.5*	0.84
	her1.7	0.84
	her2.0	0.84

Table 4: Main detector acceptances for the $E_{FCAL} > 1$ GeV Monte Carlo models. The nomenclature is explained in the text.

Model	Fractions f_i	χ^2_{fit}	χ^2 E_{FCAL}	χ^2 E_{BCAL}	χ^2 E_{RCAL}	χ^2 E_T	Acc.
soft0.41	0.16						
pyt1.8	0.70	3.3	3.4	3.2	2.6	9.1	0.85
diff	0.14						
soft0.41	0.21						
pyt2.0	0.66	2.2	2.3	2.1	3.8	8.1	0.86
diff	0.13						
soft0.41	0.21						
her1.5	0.73	4.6	2.5	8.0	5.5	3.0	0.83
diff	0.06						
soft0.41	0.20						
her1.7	0.73	4.2	3.0	5.8	6.6	2.2	0.83
diff	0.07						
soft0.41	0.32						
her2.0	0.62	3.9	3.3	4.7	3.9	2.0	0.84
diff	0.06						
pytlow	0.92	2.7	2.6	2.8	3.2	2.3	0.86
diff	0.08						
herlow	1.00	2.3	1.3	3.9	2.2	1.0	0.95
diff	0.00						

Table 5: Results of the fits of the fractions of subprocesses for the $E_{FCAL} > 1$ GeV sample.

Subprocess	Acceptance
$\gamma p \to Vp$	0.31 ± 0.04
$\gamma p \to VX$	0.37 ± 0.04
$\gamma p \to Xp$	0.80 ± 0.05
$\gamma p \to XX$	0.88 ± 0.08

Table 6: ZEUS acceptances for the individual subprocesses for $E_{FCAL} < 1$ GeV.

Subprocess	Events	Fraction	Acceptance
Total	$7582 \pm 190 \pm 510$	100%	$76 \pm 5\%$
Non-diffractive	$4852 \pm 72 \pm 270$	$64.0 \pm 0.9 \pm 3.6\%$	$90 \pm 3\%$
Inelastic diffractive	$1766 \pm 113 \pm 356$	$23.3 \pm 1.5 \pm 4.7\%$	$63 \pm 8\%$
Elastic	$964 \pm 203 \pm 326$	$12.7 \pm 2.7 \pm 4.3\%$	$27 \pm 4\%$

Table 7: Corrected numbers of events, event fractions and acceptances for the different photoproduction processes.

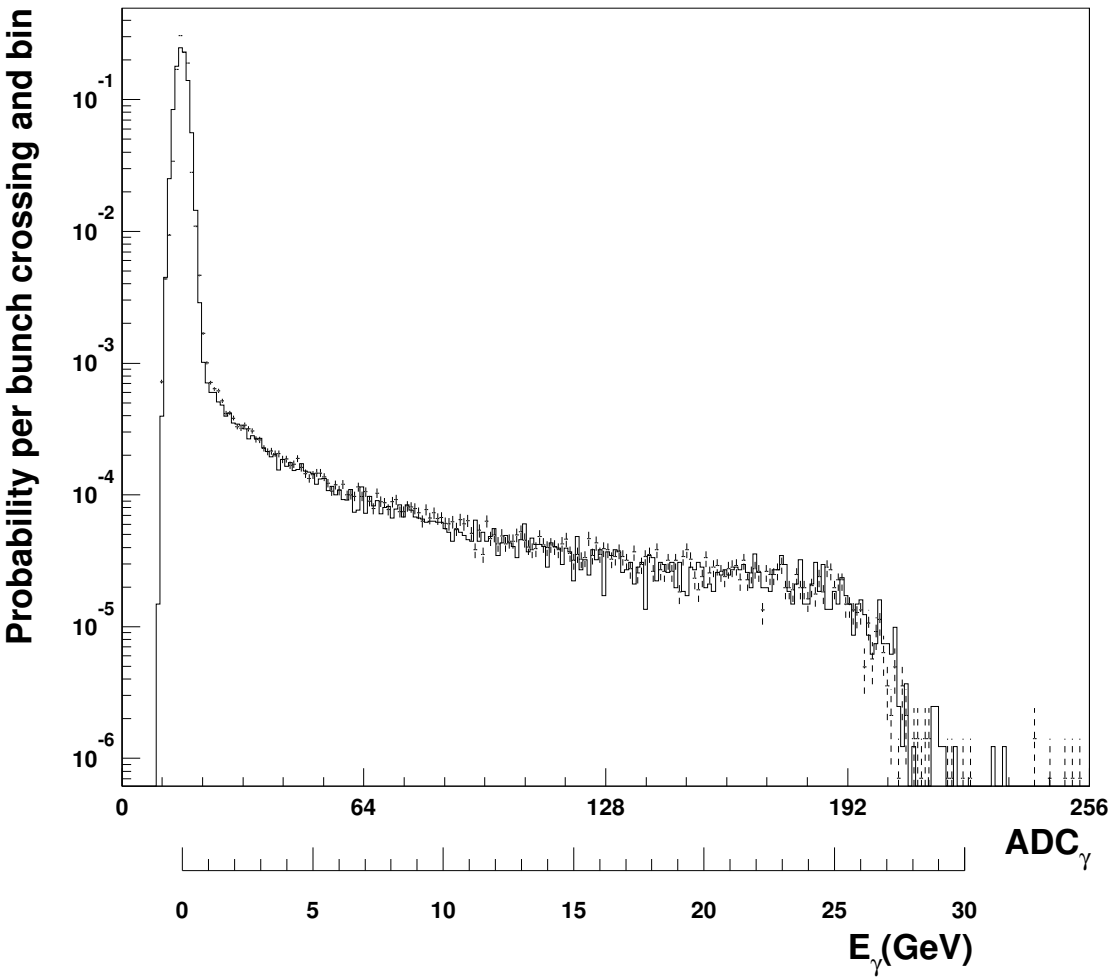

Figure 1: Measured (dashed error bars) and simulated (solid line) bremsstrahlung spectrum in ADC counts and GeV.

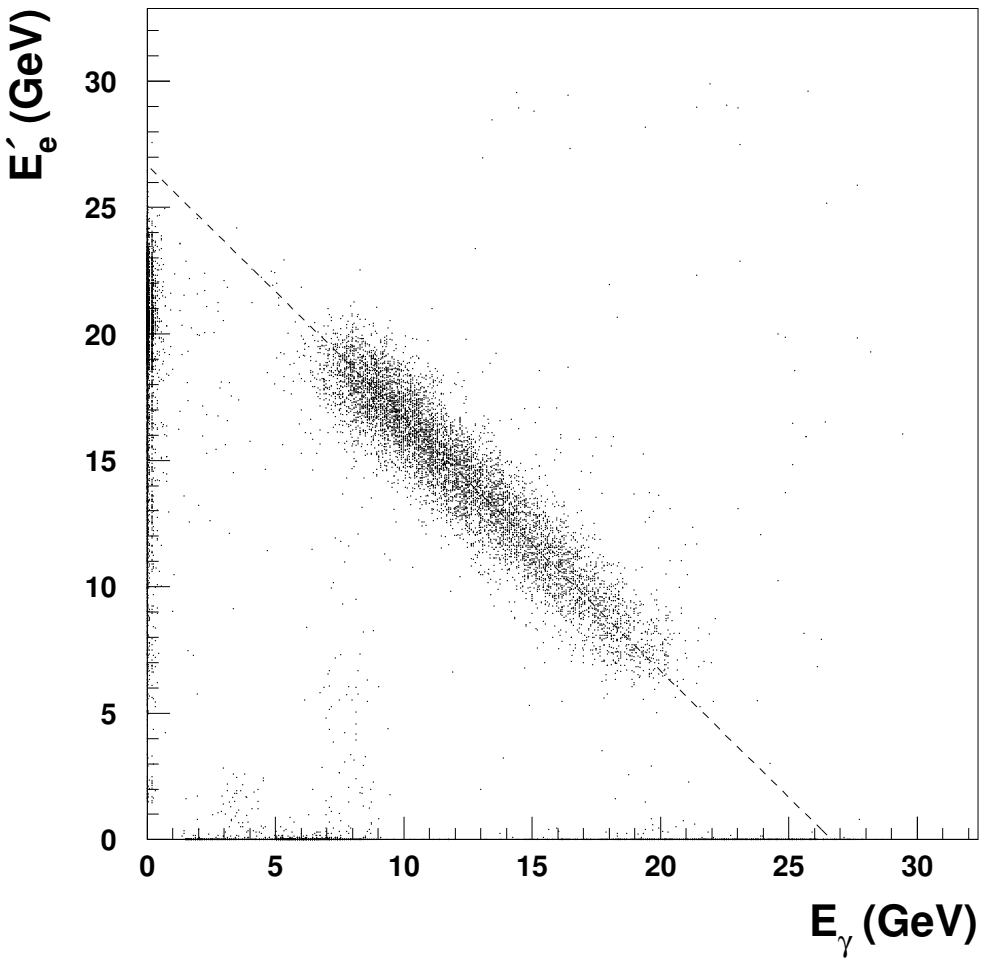

Figure 2: Correlation plot of the measured electron (E'_e) and photon (E_γ) energies for random bunch crossings (events with electron and photon energies lower than 3 GeV were rejected at the trigger level). The dashed line corresponds to the total energy, $E'_e + E_\gamma$, being equal to the electron beam energy $E_e = 26.7$ GeV.

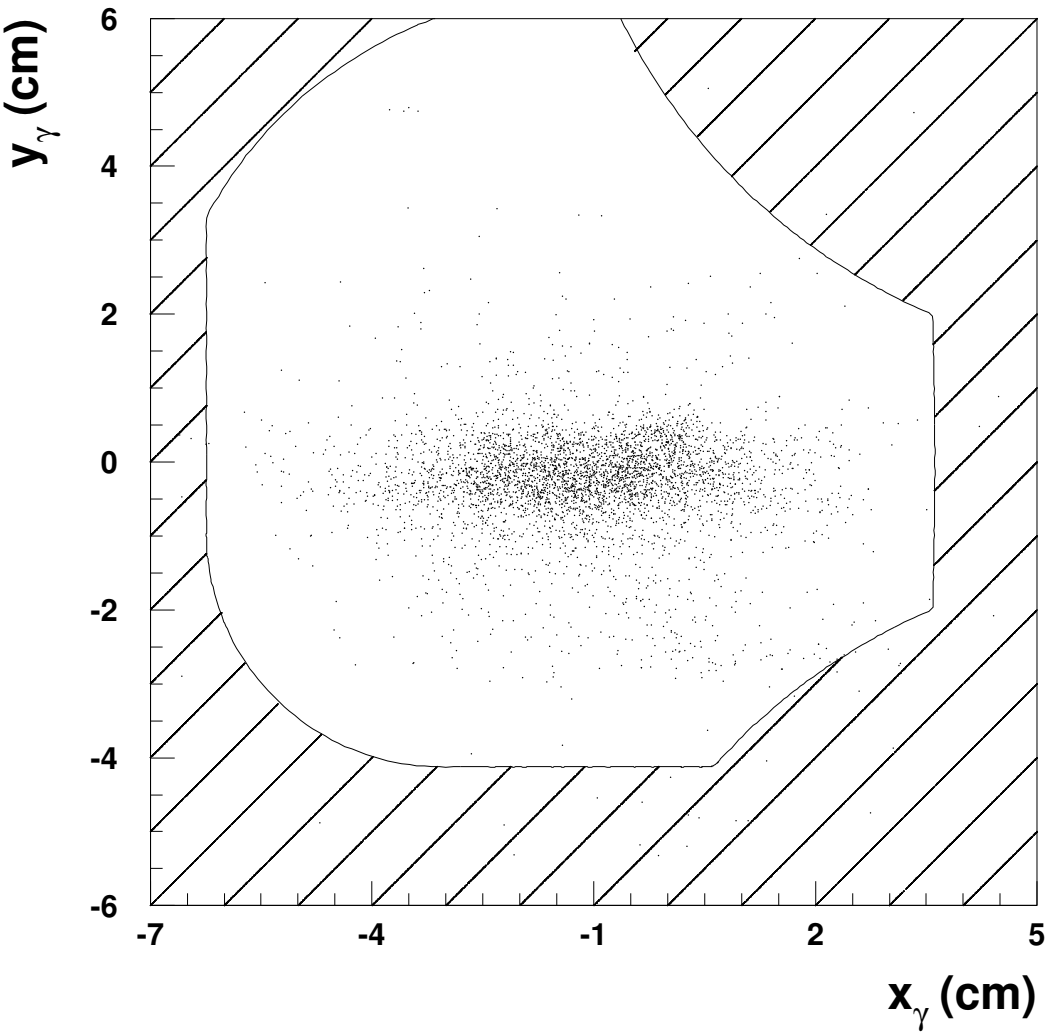

Figure 3: Photon beam profile measured in the photon calorimeter. The hatched area marks regions at the calorimeter face shadowed by the beam-line magnets.

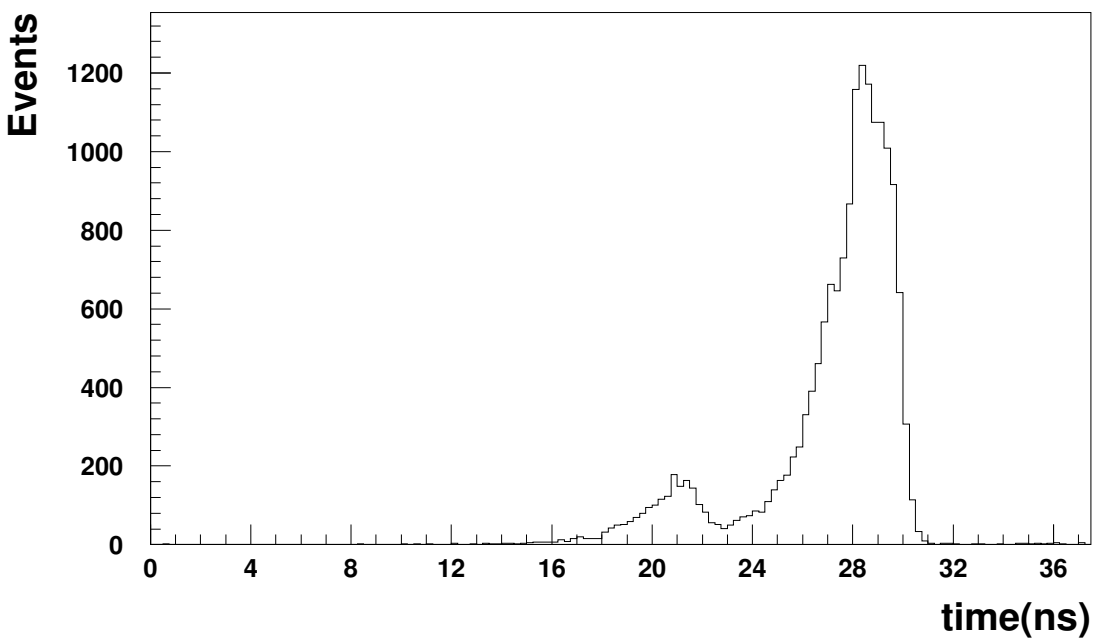

Figure 4: Time spectrum of the signals of main and satellite electron bunches measured by the C5-Counter. Smaller time values correspond to later arrivals at the C5-Counter.

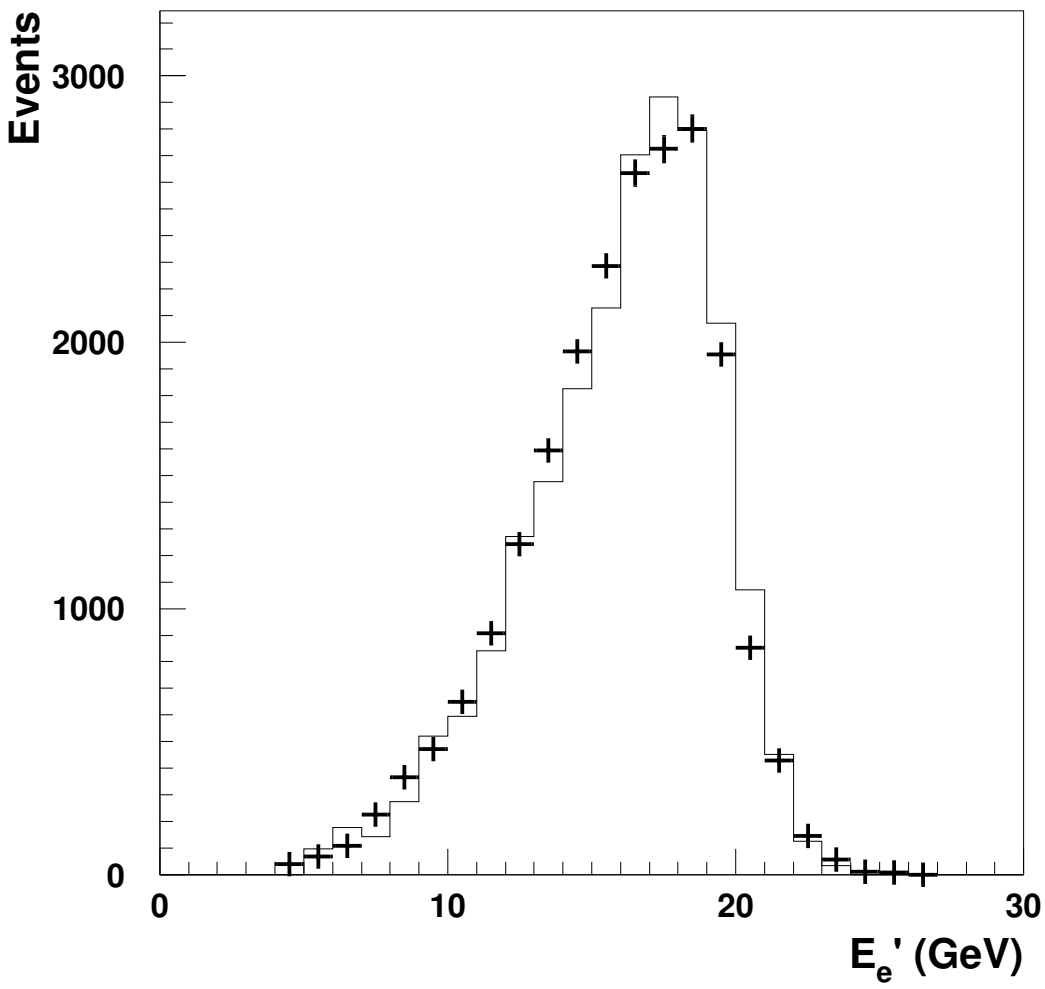

Figure 5: The measured electron spectrum of the photoproduction events in the luminosity electron calorimeter. The histogram is the expected spectrum from the PYTHIA Monte Carlo generator after correction for the detector acceptance.

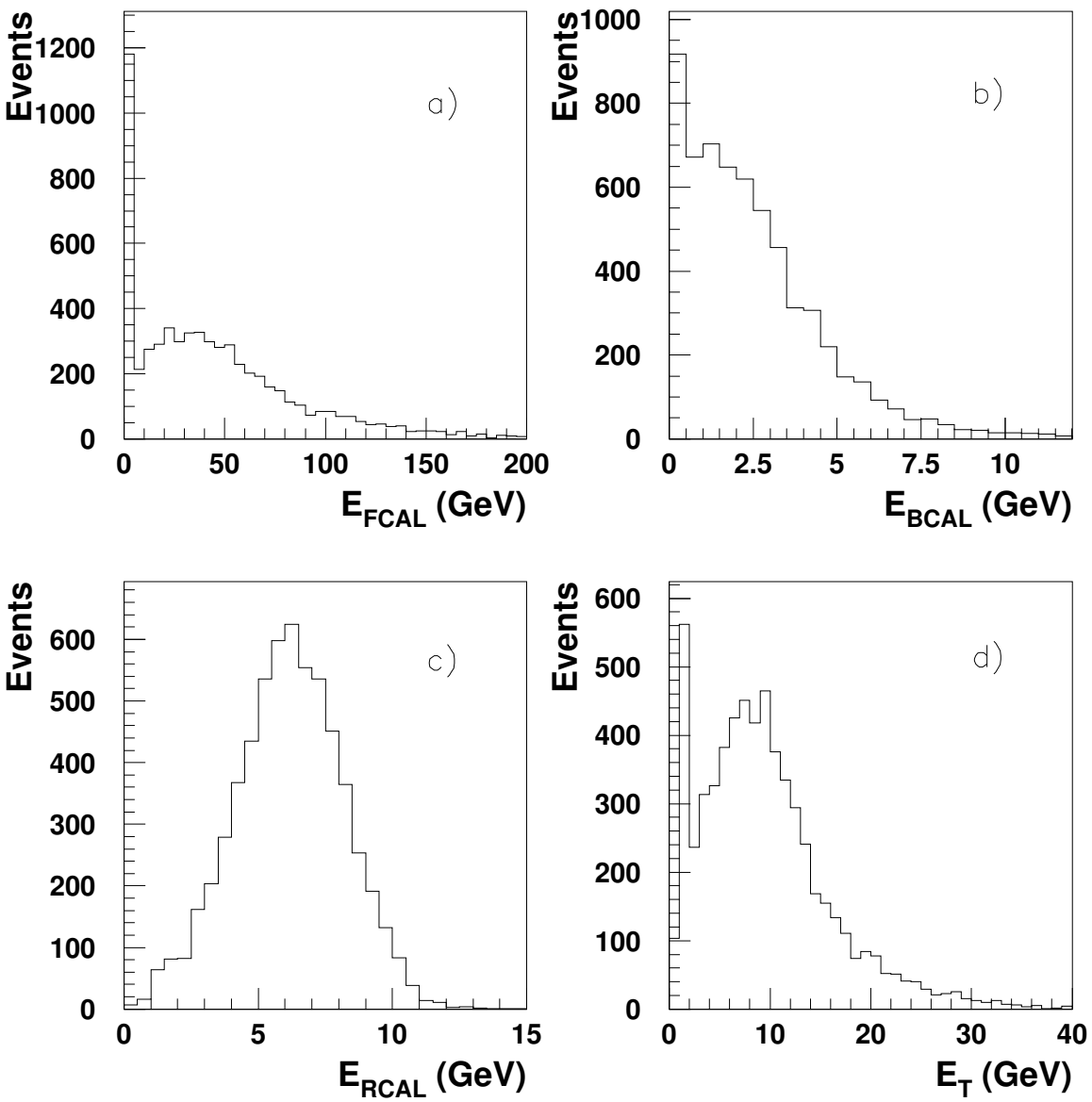

Figure 6: Distributions of event variables: a) energy in FCAL, b) BCAL, c) RCAL, and d) total transverse energy E_T for the final tagged photoproduction sample.

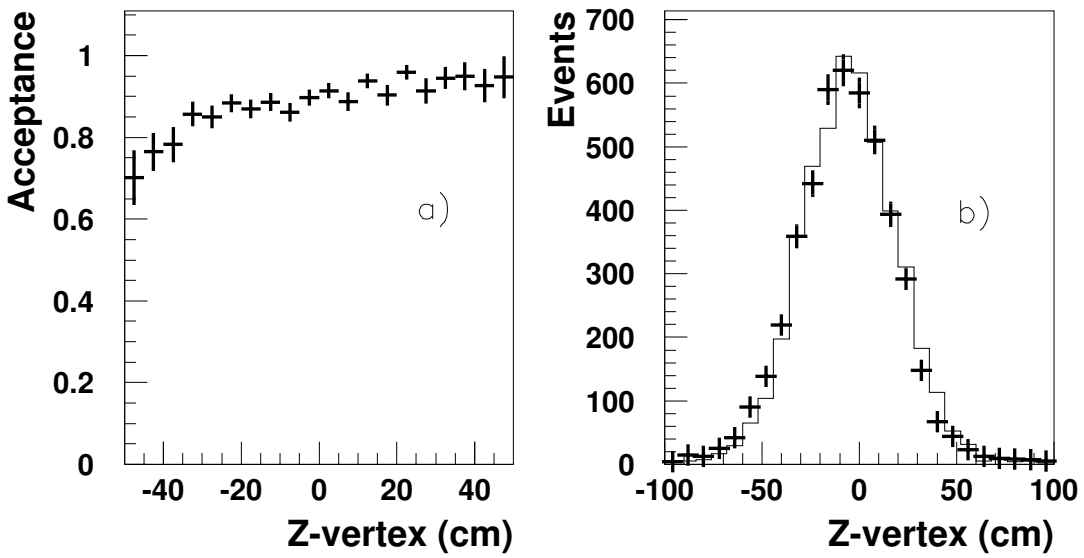

Figure 7: a) Acceptance as a function of Z-vertex for PYTHIA minimum bias events, b) comparison of the reconstructed Z-vertex distributions: experimental photoproduction sample with $E_{FCAL} > 1$ GeV (crosses), PYTHIA minimum bias events passed through the ZEUS analysis chain (solid line).

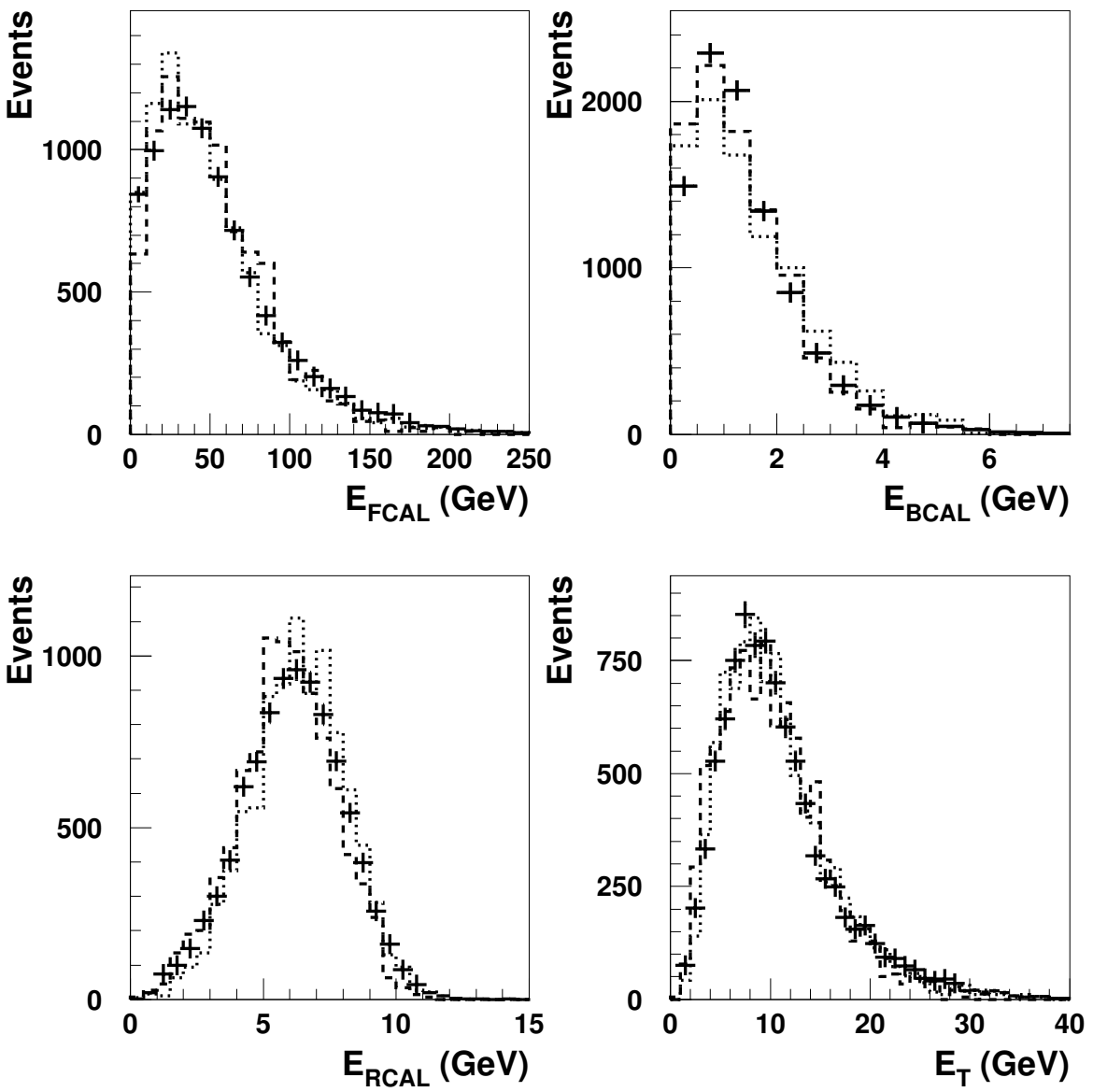

Figure 8: Comparison of the best fits to the data (crosses) for the HERWIG (dotted) and PYTHIA (dashed) minimum bias Monte Carlo samples for $E_{FCAL} > 1$ GeV.

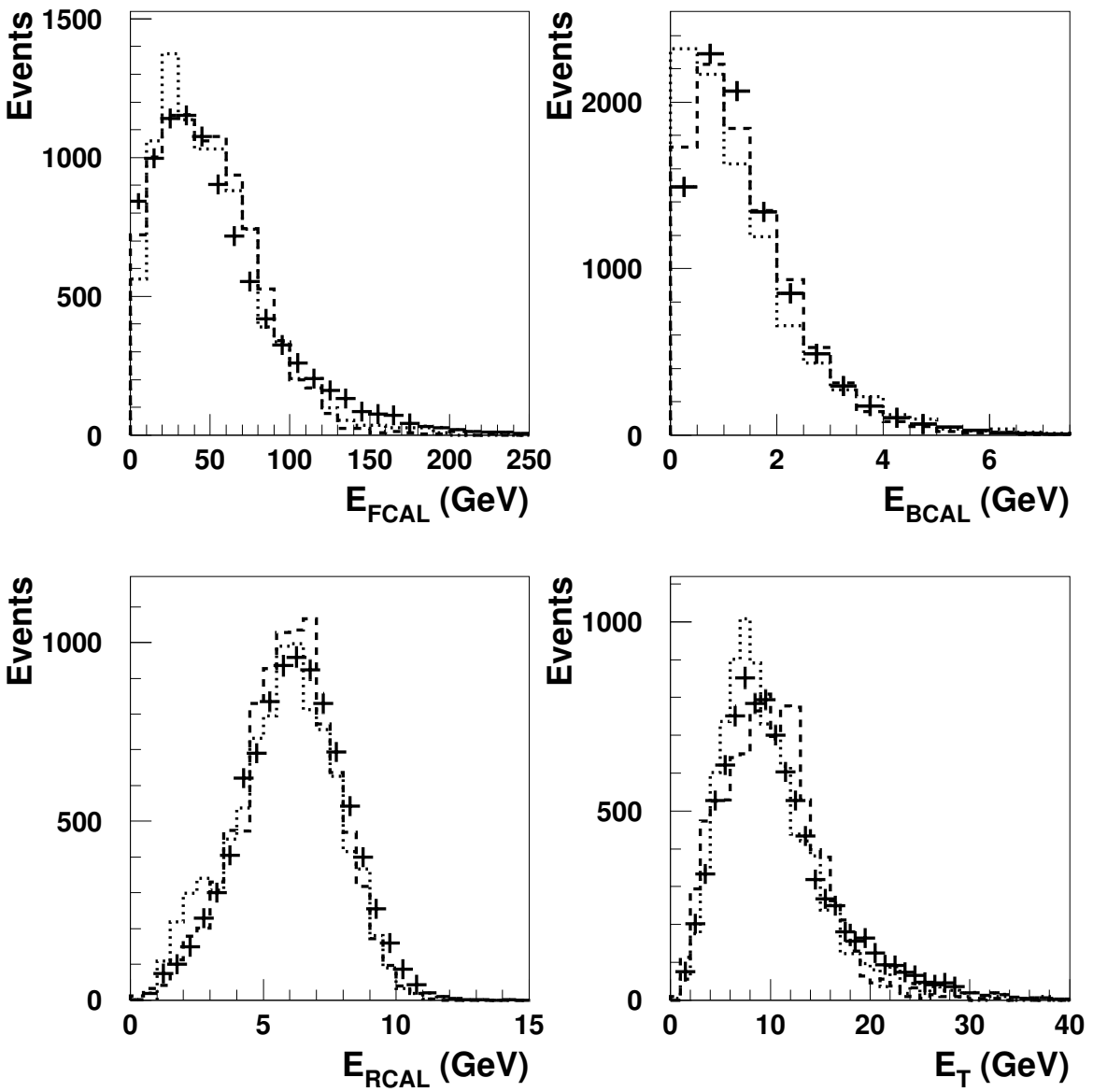

Figure 9: Comparison of the best fits to the data (crosses) for the sum of the soft component from PYTHIA and the hard components from PYTHIA (dashed - row 2 in Table 5) and HERWIG (dotted - row 5 in Table 5) for $E_{FCAL} > 1$ GeV.

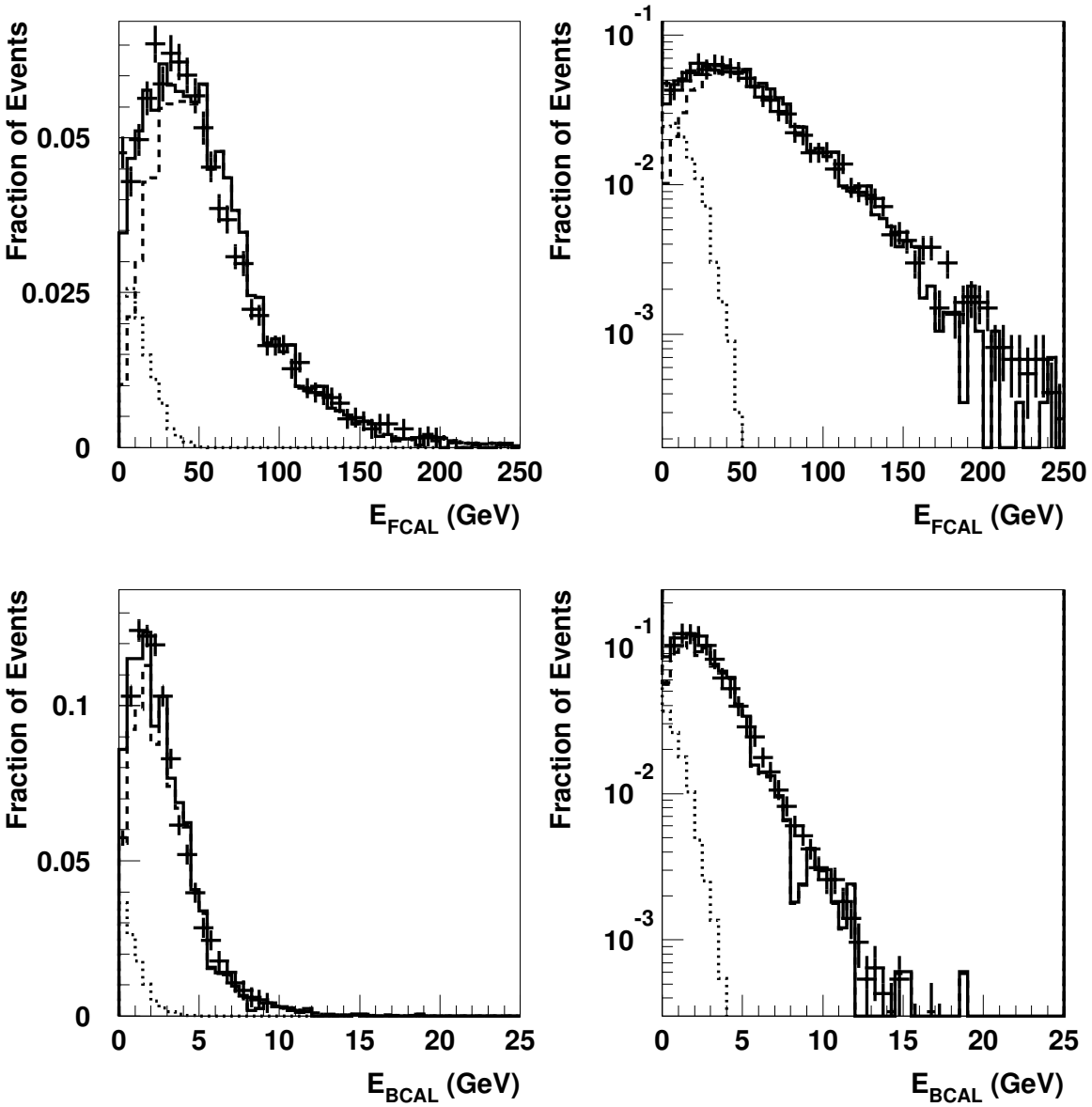

Figure 10: Comparison of the best fit to the data (crosses) for the model *pytlow* + *diff* (see text) for $E_{FCAL} > 1$ GeV. The two contributions are shown separately: *pytlow* - dashed, *diff* - dotted line. The histograms of E_{FCAL} and E_{BCAL} are plotted in a linear scale on the left side and in a logarithmic scale on the right side.

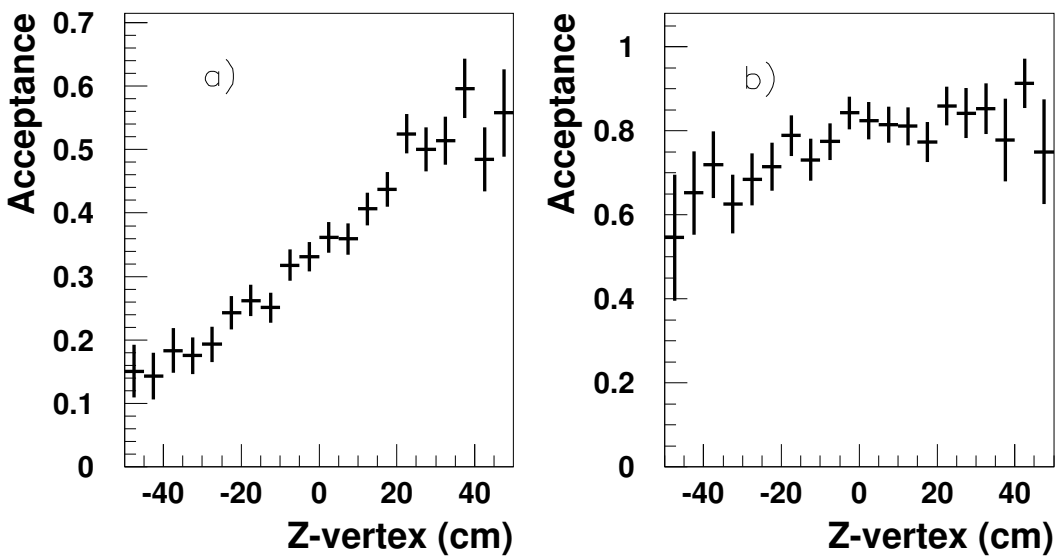

Figure 11: Acceptance as a function of Z-vertex for a) PYTHIA elastic vector meson production, b) PYTHIA photon diffraction.

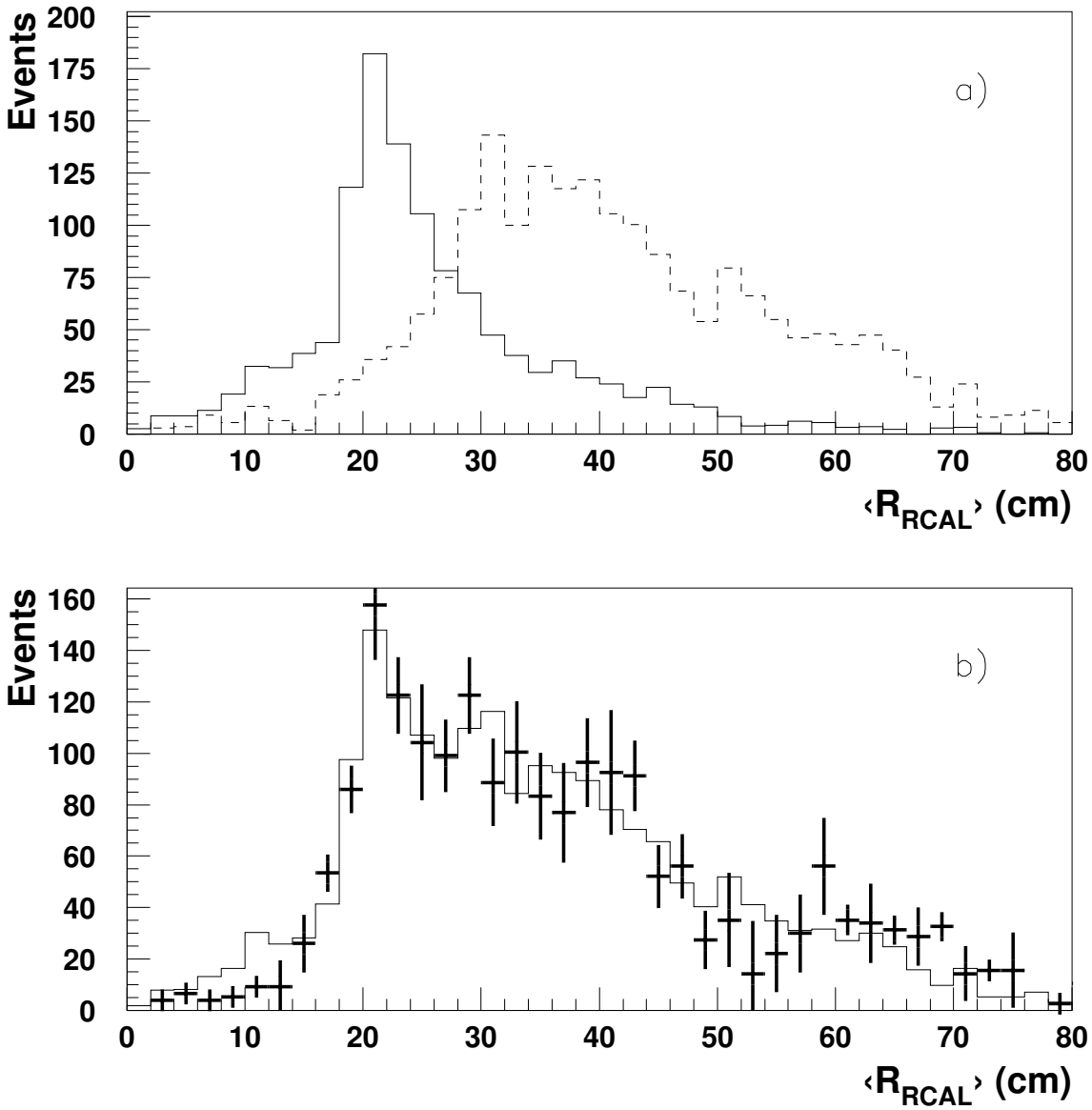

Figure 12: The energy weighted radius in RCAL, $\langle R_{RCAL} \rangle$, for: a) the PYTHIA Monte Carlo prediction of the Vp component (solid line) and of the Xp component from the Nikolaev-Zakharov model (dashed line), b) data (crosses) compared to the best fit sum of Vp from PYTHIA and Xp from the Nikolaev-Zakharov model for $E_{FCAL} < 1$ GeV.

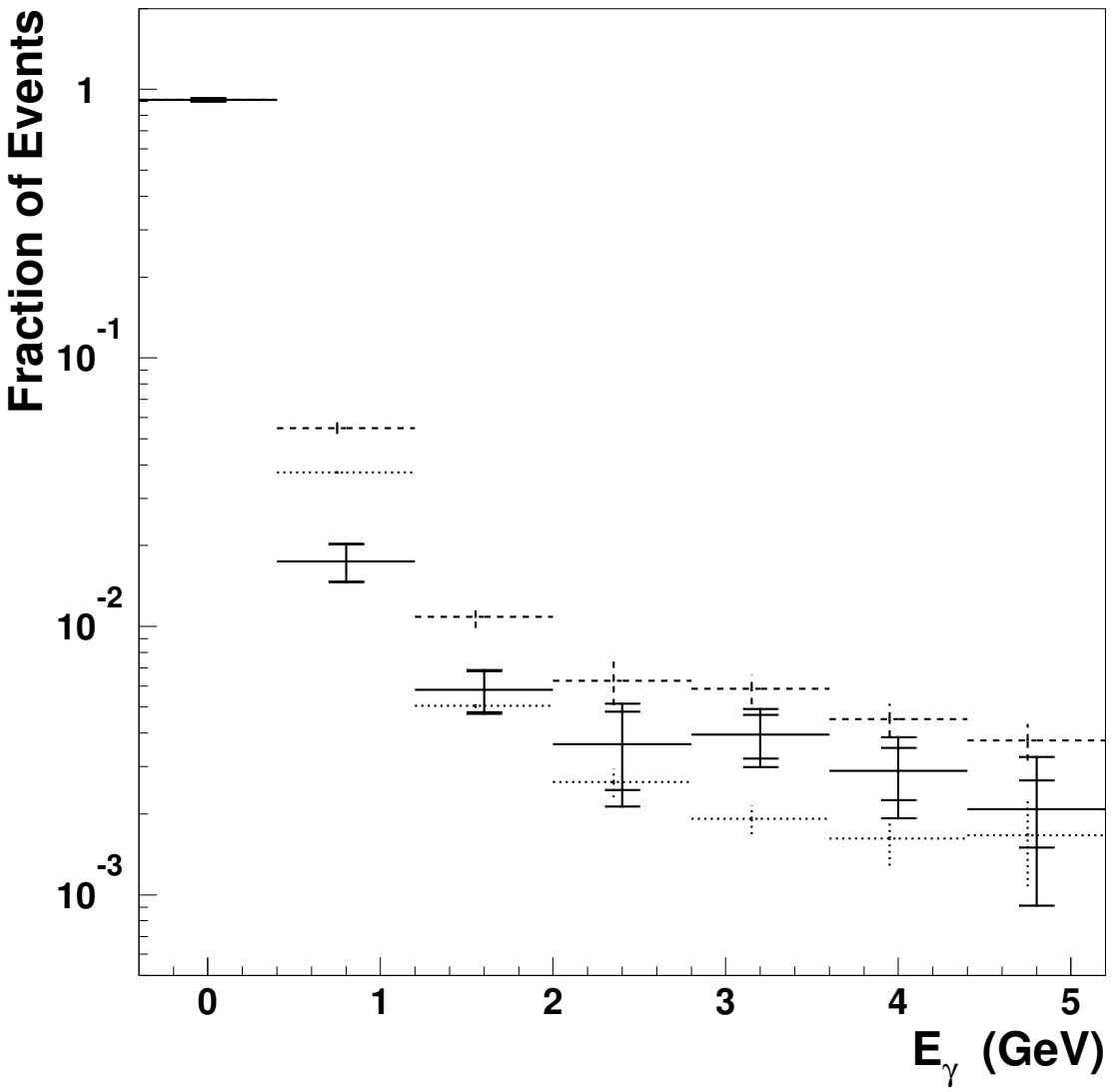

Figure 13: The experimental spectrum of photon energies measured in the photon calorimeter. The distributions show the fraction of events with a given photon energy; all spectra are normalized to one. The dashed line is the spectrum from the photoproduction sample without the $E_\gamma < 1$ GeV cut and the dotted one is background determined from random bunch crossings. The difference of the two spectra (solid line) is the experimental spectrum of accepted radiative photons. Statistical (inner) and systematic (outer) errors are shown separately.

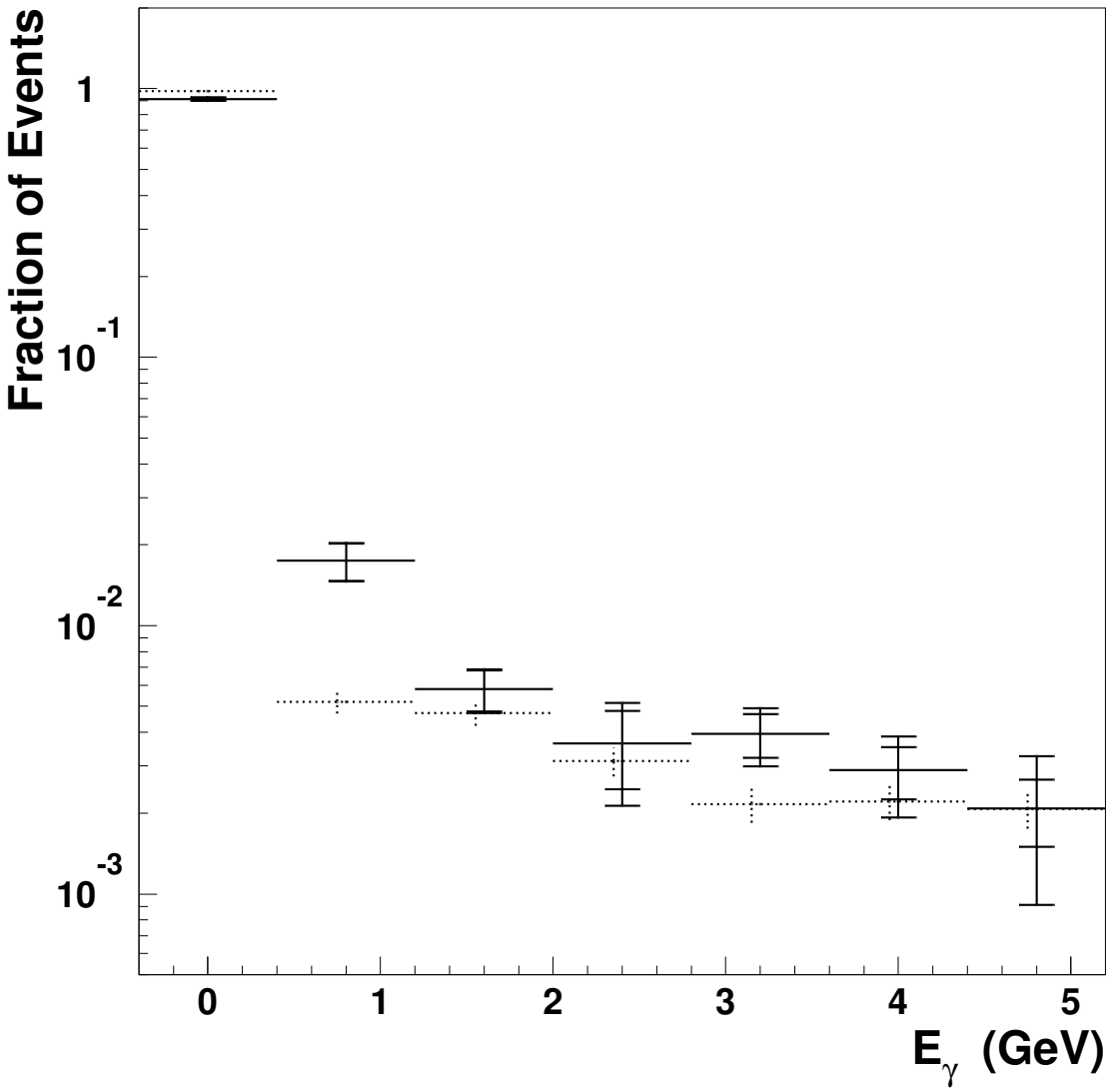

Figure 14: The experimental spectrum of radiative photons (solid line) compared to the Monte Carlo prediction (dotted). The experimental spectrum including its statistical (inner) and systematic (outer) errors, has been taken from Fig. 12. For the Monte Carlo spectrum only statistical errors are shown.

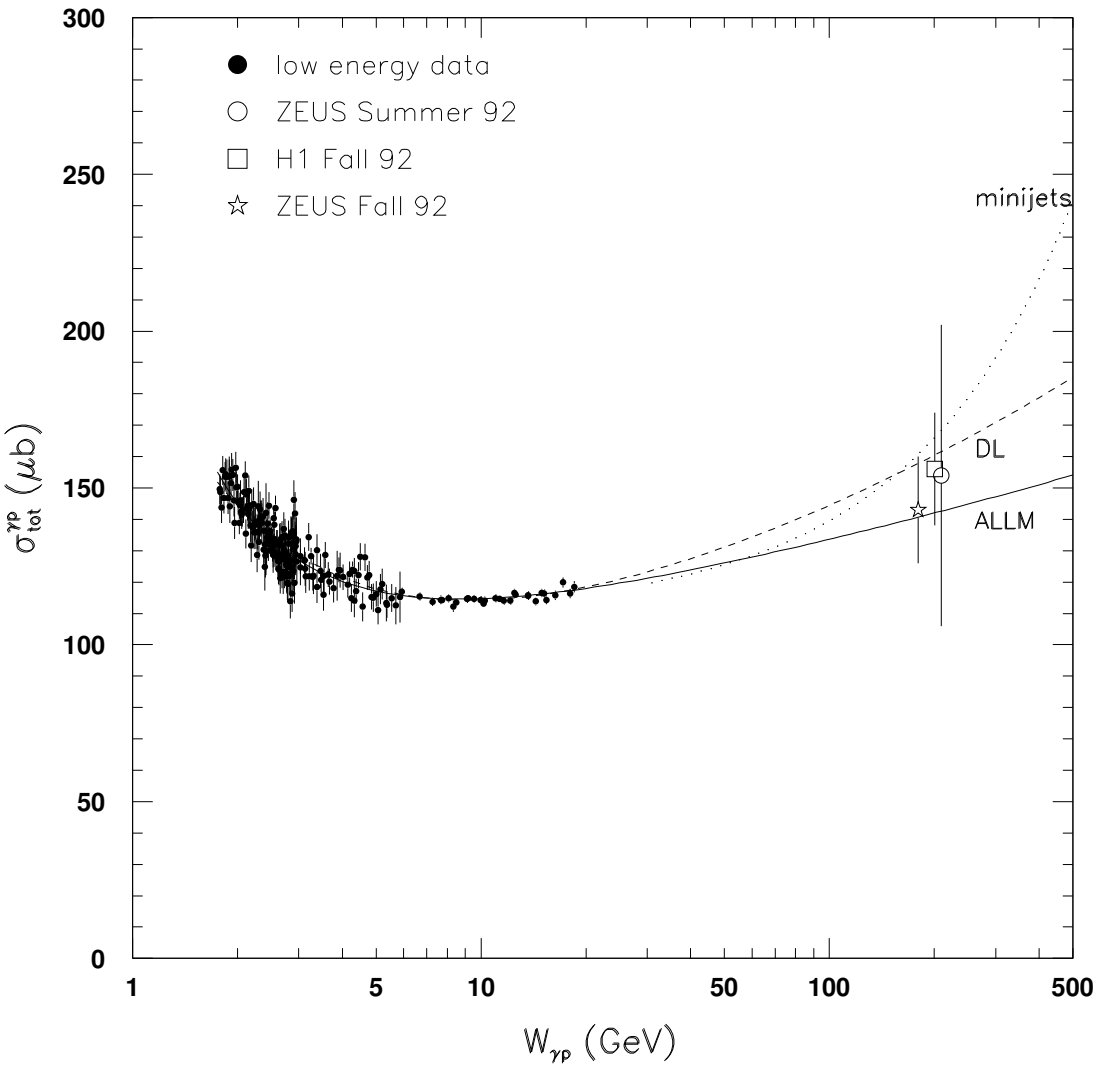

Figure 15: Total photoproduction cross section as a function of the γp center of mass energy $W_{\gamma p}$ (references for the data • – [3], ○ – [1], □ – [2]). The solid line is the prediction of the ALLM parametrization, the dashed line is that of DL, and the dotted line uses the DG parametrization for the photon with $p_t^{min} = 2$ GeV.

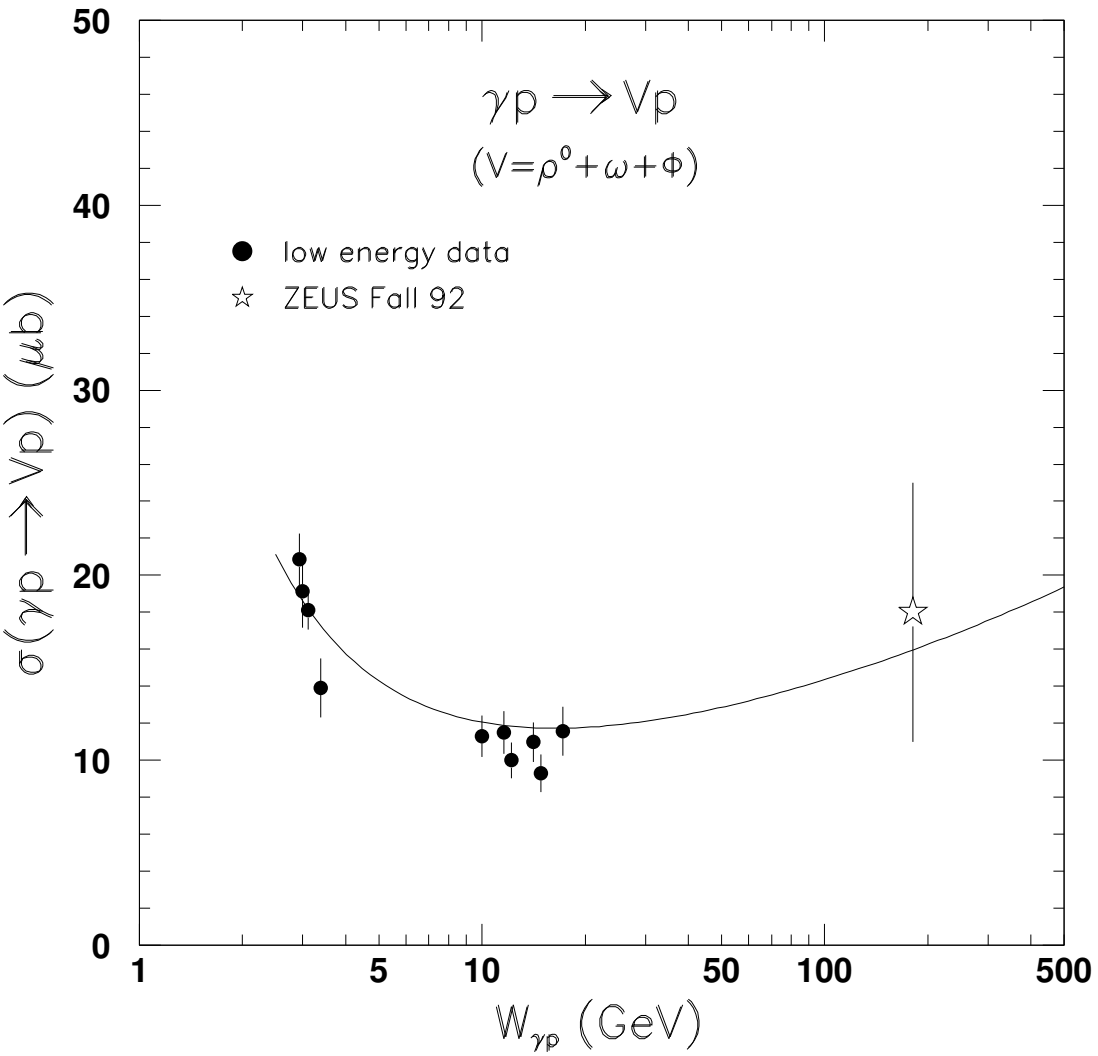

Figure 16: Cross section for the reaction $\gamma p \to Vp$ as a function of the γp center of mass energy $W_{\gamma p}$ (references for the data • – [35]). The curve is taken from ref. [32].